Review

Recent Advances in Noble Metal Nanoparticles for Cancer Nanotheranostics

Dhiraj Kumar [1,*] **, Isha Mutreja** [2] **and Ajeet Kaushik** [3,*]

1   Division of Pediatric Dentistry, School of Dentistry, University of Minnesota, Moos Health Science Tower, 515 Delaware Street S.E., Minneapolis, MN 55455, USA
2   Minnesota Dental Research Center for Biomaterials and Biomechanics, Department of Restorative Sciences, University of Minnesota, Moos Health Science Tower, 515 Delaware Street S.E., Minneapolis, MN 55455, USA; imutreja@umn.edu
3   NanoBioTech Laboratory, Department of Environmental Engineering, Florida Polytechnic University, Lakeland, FL 33805, USA
*   Correspondence: kumard@umn.edu (D.K.); akaushik@floridapoly.edu (A.K.)

Abstract: The limitations of current treatment strategies for cancer management have prompted a significant shift in the research and development of new effective strategies exhibiting higher efficacy and acceptable side effects. In this direction, nanotheranostics has gained significant interest in recent years, combining the diagnostic and therapeutic capabilities of nanostructures for efficient disease diagnosis, treatment, and management. Such nano-assisted platforms permit the site-specific release of bioactive cargo in a controlled fashion while permitting non-invasive real-time in situ monitoring. A plethora of materials has been developed as pharmacologically relevant nanoformulations for theranostic applications ranging from metallic to lipid and polymer-based composite systems, with each offering potential opportunities and its own limitations. To improve advancements with better clarity, the main focus of this review is to highlight the recent developments focusing on using different noble metal nanoparticles (noble MNPs) as cancer nanotheranostic agents, highlighting their properties, advantages, and potential modifications for their successful utilization in personalized medicine. The advantage of using noble metals (not all, but those with an atomic number ≥ 76) over metal NPs is their tendency to provide additional properties, such as X-ray attenuation and near-infrared activity. The combination of these properties translates to noble MNPs for therapeutic and diagnostic applications, independent of the need for additional active molecules. Through this review, we highlighted the potential application of all noble MNPs and the limited use of osmium, iridium, palladium, rhodium, and ruthenium metal NSs, even though they express similar physicochemical characteristics. The literature search was limited by PubMed, full-text availability, and studies including both in vitro and in vivo models.

Keywords: nanoparticles; cancer; tumor; nanomedicine; noble metal; diagnostics; nanotherapeutics; nanotheranostics

1. Introduction

Cancer is a disease that presents itself as an uncontrolled growing mass or tissue and has been the second leading cause of death in the world. Billions of dollars are spent on the treatment and diagnosis of the disease annually for a better life for patients after cancer therapy [1]. In addition, a significant amount of money is invested in research to understand the reason or factors leading to the start of cancer/tumor. Furthermore, knowledge about the progression invasion of diseases to other healthy organs can play a critical role in deciding the treatment profile. Such investigations have led to the development of cancer treatment strategies essentially constrained by various factors, such as non-specific and less availability of drugs clinically (below the therapeutic window), drug resistance in general as well as against metastatic disease, and the inability to cross biological barriers [2–4].

Formulations with the potential to monitor and provide crucial information in real time about the dose, availability, and progress of treatment would help develop patient-specific therapeutic strategies [5]. This would relieve the burden of overdosing on a patient with a drug, leading to related side effects as well as the economic burden placed on the patient and the financial system.

The term "theranostics" was first introduced by John Funkhouser in 2002 for the applied application of nanoparticles in personalized medicine [6]. However, owing to technological limitations, the therapeutics and diagnostics fields have been working and progressing independently. However, with the advancements in the field of nanomedicine, there has been a growing interest in joining the two streams in the last two decades. The research field of nanotheranostics is ready to bloom and is not far-fetched. The nanotheranostics field combines three key research areas, including nano-particle/structure–organic and inorganic, therapeutics–drug/molecular delivery, and diagnostics–imaging/detection for early diagnosis, treatment, and prognosis for a specific disease type, including cancer/tumor [7–9]. Hence, nanotheranostics provides advantages over traditional treatments by delivering therapeutic molecules and providing early disease diagnosis and progression for future treatment profiles. Furthermore, targeted delivery minimizes exponential drug use/overdose and limits the socioeconomic burden as well as the real-time monitoring of payload delivery, bioavailability, and bio-distribution in patients [5,10].

Depending on the target disease type and/or molecular profile of the altered phenotype, the chemical constructs or archetypical design can be tailored for personalized strategies. Such a chemical construct includes targeting ligands for selective binding, therapeutic molecules as potential drugs, and diagnostic agents for non-invasive imaging. The additive protective-polymer coating for stability and or additional functional groups for differential bio-conjugation can be tailored for a stable multifunctional approach [4,11–14]. Among the different types of nanoparticles, metal nanoparticles provide several advantages, like controlled smaller size, high surface-area-to-volume ratio, and optical-electrical properties. Owing to the properties of nanostructures, cancer therapy has become the standard of care for cancer nanotheranostics. However, noble metal nanoparticles or nanostructures have certain advantages, such as an uncomplicated chemical synthesis profile with easy-to-tune surface conjugation, which translates to high stability [15]. These properties of the noble metallic NPs make them highly favorable for biomedical, bioactive applications, and biosensing based on various colorimetric, immune, and Raman spectroscopy assays [16].

Imaging modalities such as magnetic resonance imaging (MRI), positron emission tomography (PET), X-ray computed tomography (CT), photoacoustic tomography (PAT), magnetic resonance spectroscopy (MRS), single-photon emission computed tomography (SPECT), fluorescence imaging, and more novel spectral photon-counting CT imaging are integral parts of medicine or therapeutic processes [13,17–19]. These imaging technologies help with diagnosis (initial disease detection, progression, or suppression); however, these modalities have limitations like low resolution, sensitivity, high cost, and high radiation exposure. In addition, with traditional contrast agents, the real-time disease diagnosis and progression are far-fetched. However, with the introduction of nanoparticulate formulations as contrast agents, disease site imaging and biodistribution of the payload are possible using both current and futuristic imaging technologies. In efforts to employ noble metal NPs for non-invasive imaging and transition towards personalized nanotheranostic treatment models, the multi-functionality potential of surface-engineered noble metallic NPs is required and must be exploited. Metallic or noble MNPs have been extensively studied for both cancer therapeutic and diagnostic applications in the last decade [1,7,20].

Therefore, this review focuses on the advancements made by noble metal nanoparticles in the field of nanotheranostics in the last 10 years (literature search was performed using the PubMed website (indexed: metal nano and cancer and theranostic) and only publications with full-text availability and investigating both in vitro and in vivo models were included) (Shown in Figure 1A). We outline the different types of noble metal-based nanostructures being investigated and developed for both therapeutic and diagnostic ap-

plications in different cancer treatments. We provide details about the shape of the particles and the type of molecular conjugation to the surface for targeting cancer in in vitro and/or in vivo models. We also focused on the imaging modalities utilized for the diagnosis of the diseases in the in vivo models. Figure 1B is a schematic of an engineered smart nanoparticulate system employed for cancer targeting, monitoring and management.
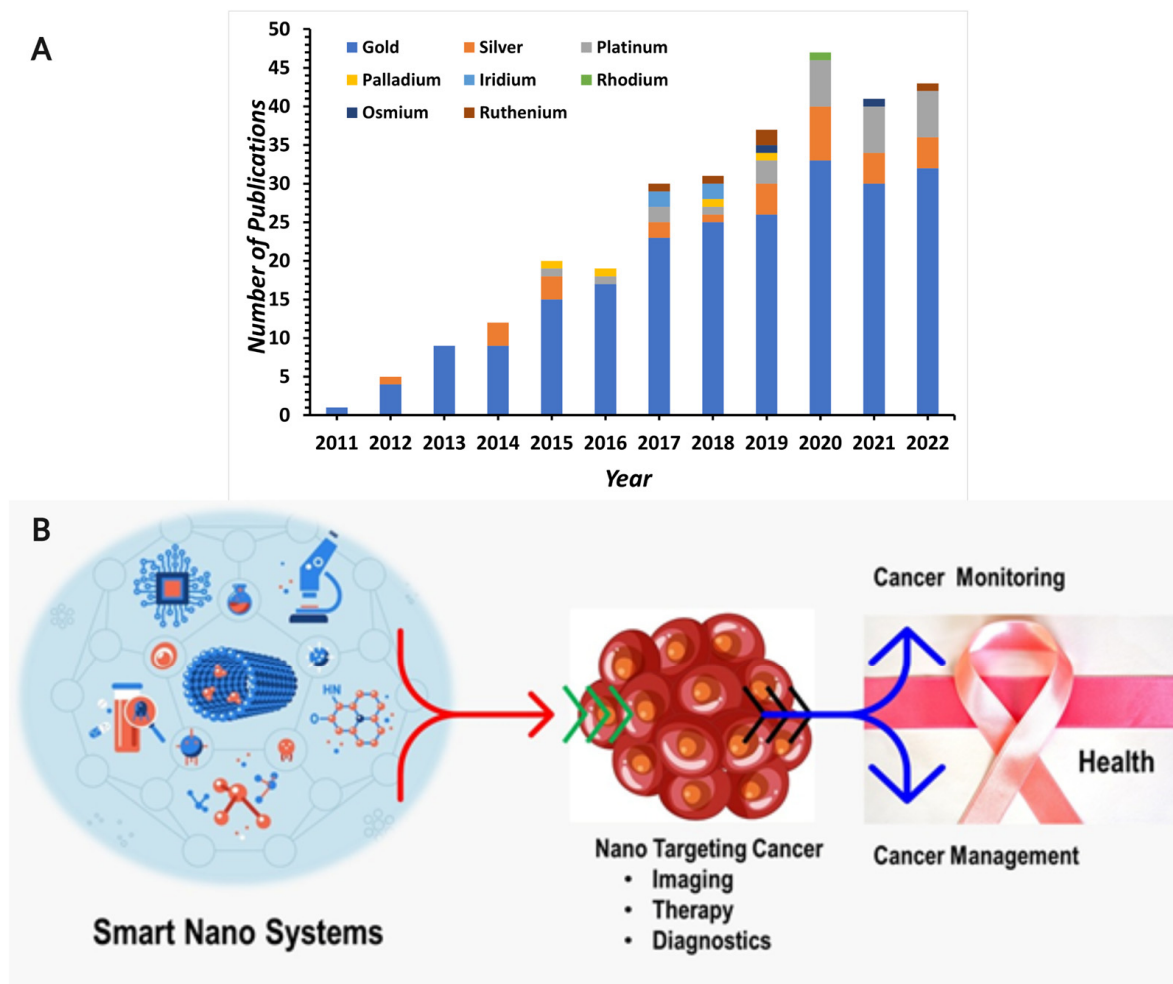

Figure 1. (**A**) Represents the number of publications for each noble metal type during the respective year. (**B**) Schematic representation of engineered smart nanosystems and their scope in cancer targeting and diagnosis.

2. Gold (Au) Nanostructures

During the last decade, several nanostructure-based platforms have been introduced for biological and device applications. These nanoplatforms include both organic NPs like polymeric, liposomes, and dendrimers and inorganic NPs such as metal, metal oxide, and silica. Among these nanostructures (NSs), Au-NSs (particles, rods, stars, and pyramids) have great potential and have been explored as multifaceted tools for different biological and biomedical applications [17,21–23]. Properties such as a high surface-to-volume ratio, inert nature but a high affinity for sulfur and amine groups for selective conjugation of polymers, peptides, and drug molecules, biocompatibility for biological applications, and optical and plasmonic properties make Au NSs highly favorable for therapeutic and diagnostic applications [24]. Furthermore, additional properties such as the Raman signal enhancer resulting from the Surface Plasmon Resonance (SPR) phenomenon, have been exploited for cancer biomarker detection and biosensing [21,25,26].

The gold nanoparticles (AuNPs, 91 nm) stabilized with thiol-polyethylene glycol (HS-PEG, 5000 g/mol) and carboxyl-PEG (HS-PEG-COOH), conjugated with 3.3′-Diethylthiatricarbocyaniniodid (DTTC) a Raman reporter molecule as well Cetuximab as EGFR blocker successfully targeted the EGFR receptor in vitro in human colorectal adenocarcinoma cells and in vivo to inhibit tumor progression along with simultaneous spectroscopic detection [21]. Figure 2A,B shows the physiochemical characterization of Au NPs, followed by confocal imaging of adenocarcinoma cells incubated with NPs (Figure 2C–E) and the Raman spectra of drug-conjugated AuNPs (Figure 2F). Figure 2G–I show an in vivo model injected with NPs and the accumulation of NPs in tumors and other organs, as confirmed by photon flux imaging. Figure 2J–L represent the histological data for the tumor tissue (Figure 2A–L). A similar formulation with 25.0 nm gold nanoparticles conjugated with VHH-122 or C225 as targeting antibodies was successfully taken up by A431 cells in vitro. The Au NPs uptake for lung cancer cells targeting was assisted by EGFR overexpression in A431 cells. The study reported a significantly higher uptake of C225 conjugated AuNPs (compared to PEG-AuNPs and VHH-122-AuNPs) by A431 cells in vitro as well as in vivo in C57BL/6 and nude mice (with A431 subcutaneous tumor). The gold NPs uptake was quantified by inductively-coupled plasma optical emission spectroscopy (ICP-OES) and tracked by Micro CT imaging [27]. Figure 2M,N show the TEM image and hydrodynamic diameter of 'as prepared' and surface-modified AuNPs, which is followed by ICP-MS quantification of gold uptake in A431 cancer cells (Figure 2O). While Figure 2P,Q show dual-energy CT images of lung tumors, mice administered with PEG, VHH and C225 modified Au NPs and ICP-MS quantification of gold in the lung tumor (Figure 2M–Q). The potential availability of a high surface area at the molecular level gives nanostructures an advantage over the bulk state. As in previous examples, the surface was tailored with selective targeting molecules for colorectal and lung cancers. A similar approach has also been used for targeting other cancer types. Breast cancer suppression using NIR photothermal therapy (PTT) in the presence of a bouquet of 13 nm AuNPs linked with mannose-polysaccharide over 60 nm AuNPs was studied. The uptake of AuNPs by MCF-7 cells in vitro and BALB/c nude tumor mice in vivo model resulted in an increase in WTp53 protein and tumor cell death when exposed to NIR 680 nm laser for photothermal therapy and monitored by dark-field imaging [28]. In another study on a photothermal therapeutic approach for breast cancer, an AuNPs–aptamer–graphene oxide hybridized system modulated heat shock protein expression in selectively targeted MCF-7 cells in vitro [29].

Gold nanostructures such as nanopyramids conjugated with indocyanine green showed higher tumor uptake (A375 tumor mice), tumor size reduction, and mouse survival in vivo after intravenous injection after -PTT. Non-invasive dual-modalities, fluorescence (FL) and photoacoustic tomography (PAT) imaging confirmed nanopyramid uptake and tumor size reduction [23]. However, in different studies, gold nanostars that are noted as being 'as prepared', silica-coated, silver-coated, and copper-labeled are known for enhanced-tunable plasmonic (based on size) properties in the NIR field (also known as tissue optical windows) have been applied for lymphatic system mapping, live cell imaging, breast cancer, prostate cancer imaging, and brain tumor margins invasion. The imaging of these biological systems was possible using PAT, two-photon photoluminescence (TPL), PET, MRI, X-ray CT, and Surface-Enhanced Raman Scattering (SERS) imaging [17,30,31]. The nanostars were able to enhance the SERS signal up to 10^{15} fold making them a powerful tool for biomarker detection at the molecular scale in conjunction with photodynamic and photothermal therapy as a therapeutic means [18,31,32]. Conventional SERS-active molecules are constrained to thiolated (-SH) terminal groups, which have chemical stability and spectral overlap as limitations. Mingmin Li et al. introduced nitrile- and alkyne-based SERS reporter compounds for active cancer biomarker imaging both in vitro and in vivo with strong non-overlapping signals for multiplex imaging [33].
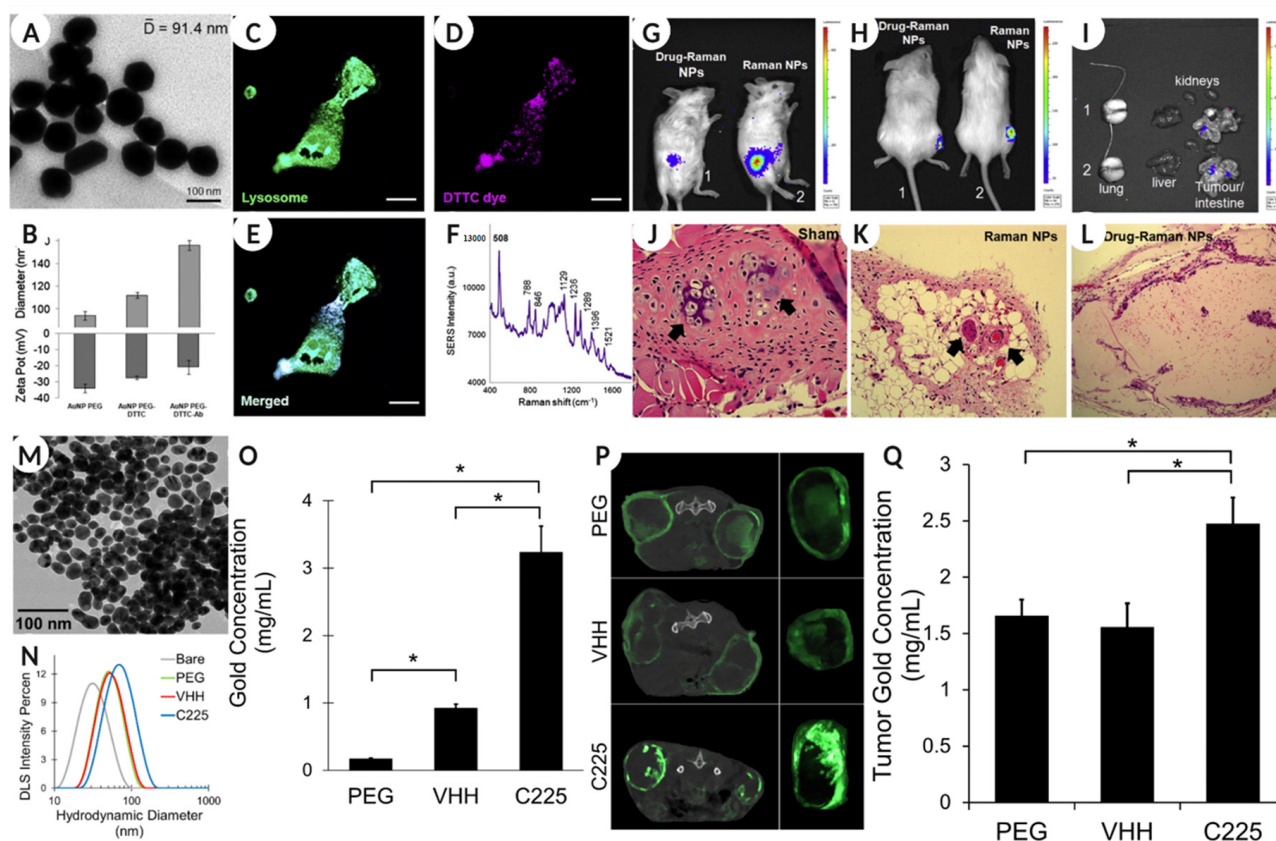
Figure 2. (**A**,**B**) The TEM shape size and hydrodynamic diameter, along with surface charge on AuNPs, while the lysosome, Raman reporter, and combined confocal image of adenocarcinoma cells are shown in (**C**–**E**). The Raman spectra and peaks of the drug–Raman AuNPs in HT-adenocarcinoma cells with SERS peak at 508 cm^{-1} shown in (**F**–**H**) represent the photon flux activity of luciferase in the tumor with NP-injected mice while (**I**) represents the activity in other organs. Images (**J**–**L**) show the hematoxylin and eosin (arrows represent tumor clones) (**H**,**E**) stain of sham-treated, AuNPs/Raman and drug–AuNPs/Raman-treated tumor; image reused with permission from reference [21]. Copyright 2014, Elsevier. (**M**,**N**) The TEM shape and hydrodynamic diameter of surface-modified AuNPs, while (**O**) shows the ICP-MS analysis of AuNPs uptake by A431 cancer cells. (**P**,**Q**) The dual-energy CT image of a lung tumor after modified AuNP administration and CT quantification of Au in an in vivo tumor model, respectively; images reused with permission from reference [27]. * $p < 0.05$. Copyright 2018, Public Library of Science (PLOS).

Even though the choice of metal nanoparticulate is important, considering the properties like biocompatibility and ease of functionalization. However, for therapeutic and diagnostic applications, the conjugation or immobilization of selective targeting biomolecule types via electrostatic or covalent bonding on the NP surface can play a significant role in the NP uptake process. The activation of the JAK/STAT3 pathway via IGF and EGFR signaling has been linked to head and neck cancer (HNC). The delivery of STAT3-oligonucleotide drug nanoconstructs, along with radiation therapy, has been reported to reduce the A431 HNC cell viability by 20% more, and a similar effect was observed in radioresistant FaDu cells [34]. Similarly, for radioimmunotherapy for a solid tumor, EGF-tagged AuNPs labeled with indium (^{111}In) successfully targeted in vitro (MDA-MB-468 and 231-H2N cells) and in vivo tumors (MDA-MB-468 or 231-H2N xenografts in BALB/c nude mice). The formulation stabilized using thiolated polyethylene glycol (HS-PEG, 6000 g/mol, ^{111}In-EGF-Au-PEG6000) and conjugated with the EGF antibody showed significantly higher uptake of AuNPs (versus ^{111}In-EGF-Au) in MDA-MB-468 xenografts when co-administered with 15 µg of non-labeled EGF compared to the 231-H2N xenograft. The study suggested that free EGF anchored at the EGFR receptors in the liver improved the systemic circulation of la-

beled AuNPs, thereby enhancing uptake in the tumor, as diagnosed by SPECT imaging [35]. A similar outcome was achieved with gold nanorods (GNRs) (96.37 nm) stabilized with fucoidan (Fu) and conjugated with anti-EGFR antibodies (MDA-MB-231 cells) [22] or conjugated with curcumin for human lung cancer, oral epidermoid carcinoma cells, and HepG2 liver carcinoma cells [36]. In another study, GNRs coated with mesoporous silica film targeted melanoma (A375 cells) tumors for therapeutic effect and were also designed for diagnosis using ultrasound and photoacoustic dual modality imaging. The study reported a reduction in tumor size 18 days after GNR injection and laser irradiation [23,37]. While in several other studies, the biomolecules like endogenous protein glutathione S-transferase (GST), a modular peptide (Pro–Asp–Trp–Glu–Gly–Pro–Glu–Arg–Asp–Lys (Cys–Cys–Tyr–C6), folic acid, miRNA, RGD peptide, and shuttle peptide-angiopep-2 have been employed for selective targeting of different cancer types; and sometimes shelled with metals like gadolinium (Gd), palladium (Pd) and iron oxide to harness their properties for nanotheranostics applications [20,38–43].

3. Silver (Ag) Nanostructures

Similar to Au nanoparticles/nanostructures, silver nanoparticles (AgNPs) also have optical, electrical, thermal, and biological properties. AgNPs also exhibit a high surface-to-volume ratio, surface plasmon resonance, absorbance at a specific wavelength, and an enhanced signal. The surface of AgNPs can be tailored to different functional groups [44]. As a result, AgNPs have been frequently exploited in medical, health care, consumer, cosmetics, textile, and food products/industries [45–47]. There is sufficient literature on antimicrobial, antibacterial, and wound-healing applications for pristine and surface-modified silver nanoparticles [38,44,45,47,48]. However, compared to gold NPs, AgNPs have not yet found their way into cancer therapeutic or diagnostic applications, as evidenced by limited studies in the last decade.

The bio-synthesized (using *Olax scandens* leaf extract) AgNPs showed biocompatibility against non-cancerous cells (HUVEC), higher antibacterial (against *E. coli*) activity and higher cytotoxicity against cancer cells (lung cancer–A549, breast cancer–MCF7) compared to chemically synthesized AgNPs ($NaBH_4$ as reducing agent) during in vitro studies [49]. Another in vitro study explored the potential of folic acid conjugation to PEG-stabilized AgNPs (70 nm) for folate receptor-positive cancer cells. The SKOV3 and L1210 cells, as well as folate receptor positive (FR+) cells, demonstrated significantly higher uptake of folic acid conjugated AgNPs compared to the folate receptor-negative cells (FR-, MES-SA, and MES-SA/Dx5), as confirmed by ICP-MS. The formulation successfully delivered the doxorubicin drug within cancer cells via a *pH-responsive* mechanism and therapeutic effect triggered by laser exposure for photodynamic therapy, suggesting the potential of dual, chemo, and photodynamic therapy [50]. Similarly, in a comparative in vitro study, 50 nm silver nanoparticles capped with PEG600 showed the effectiveness of radiation therapy (4Gy X-ray) at 0.23 μg/mL concentration against human oral cancer (KB) cell line via nucleic acid damage [51]. Contrary to pristine AgNPs, in two independent in vitro investigations, silver–gold bimetallic nanostructures were explored for targeting human cervical carcinoma (HeLa) and malignant melanoma (A375) cells. These bi-metallic nanoparticles harnessed the ability of silver to induce apoptosis by generating reactive oxygen species (ROS) and DNA damage [52]. Figure 3A–C show the luminescence spectra and TEM images of the silver–gold hybrid nanoparticles. Figure 3D–L represents the bright field and fluorescence images of HeLa cells incubated with the NPs suspension. Figure 3M,N are the TEM images showing NP uptake by cancer cells, and Figure 3O–Q are the flow cytometry analysis showing apoptotic distribution after NP exposure (Figure 3). On the other hand, gold nanoclusters are known to improve biocompatibility, stability, ease of surface conjugation, and emission in the red region, thereby generating autofluorescence. Such a formulation would be the ultimate carrier as an efficient and sophisticated smart theranostic agent [52,53].
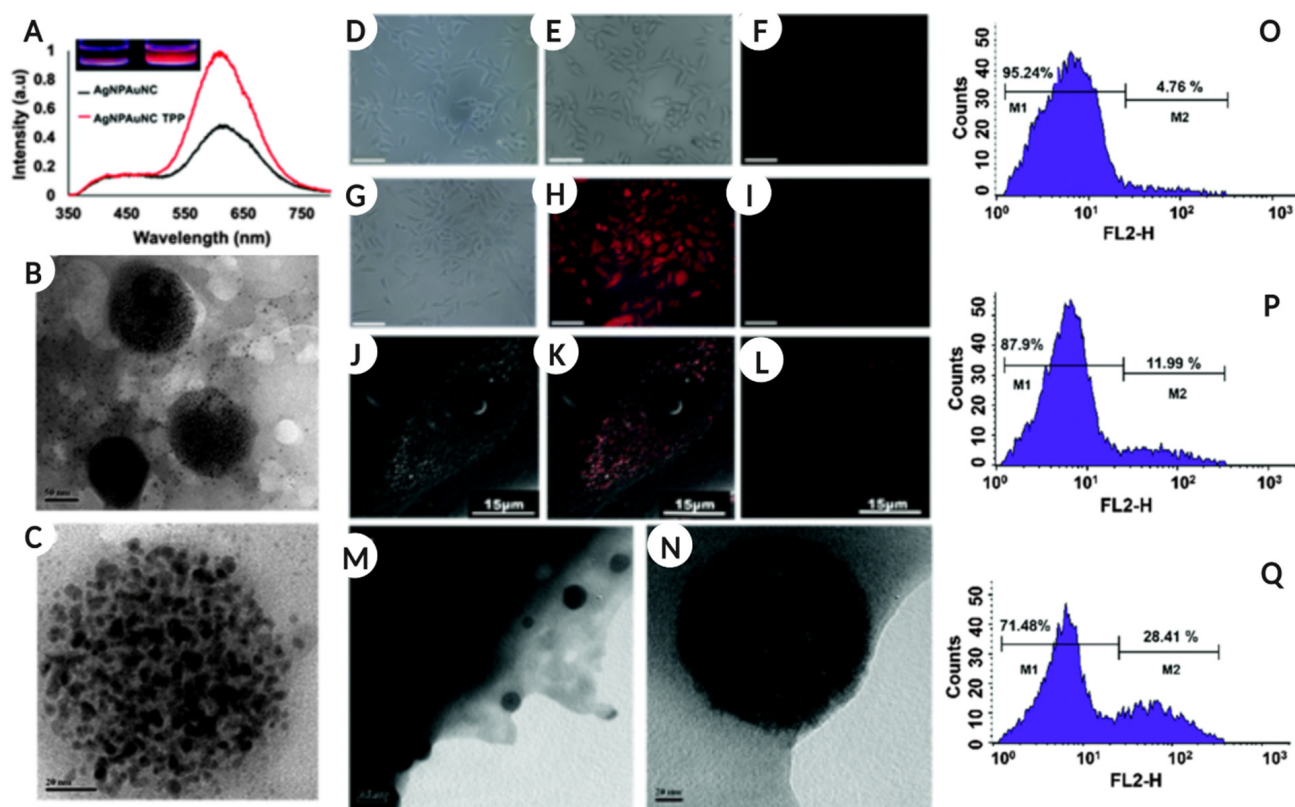
Figure 3. (**A**) The luminescence spectra of AgNPs-AuNCs, and (**B**,**C**) shows the TEM image of hybrid silver–gold nanoparticles and a high-resolution TEM image of the same, respectively. The microscopic fluorescence image of the control HeLa cells (**D**–**F**) show the bright field, fluorescent, and merged image, while (**G**–**I**) represent the same set of microscopic images post-NP treatment for 3 h. (**J**–**L**) The deconvolution fluorescence images (brightfield, fluorescent, and merged, respectively) of NP-treated HeLa cells after 3 h. (**M**,**N**) The NP internalization and high-magnification TEM images of HeLa cells with NPs. (**O**–**Q**) show the apoptosis percentage for control, AgNPs, and hybrid silver–gold NP-treated HeLa cells quantified by a Caspase 3 assay; the images are reused with permission from reference [52]. Copyright 2016, Royal Society of Chemistry.

4. Platinum (Pt) Nanostructures

Similar to the Ag nanoparticles, there is more to be discovered for platinum nanoparticles (PtNPs/Pt NPs) for theranostic applications. In contrast, there have been extensive investigations in the field of biosensing to harness the properties of pristine and Pt-other metal amalgams. This enriched biosensing research has been linked to the unique properties of Pt NPs, such as the quantum size effect, volume effect, macroscopic quantum tunneling effect, and surface effect, along with easy-to-synthesize methods for different physical and chemical properties [54,55].

Platinum NPs are known to show preferential internalization by kidney cells and rapid clearance from systemic circulation. This selective uptake of Pt NPs was used to detect acute kidney injury (AKI), which leads to inflammation and oxidative stress triggered by an excessive amount of reactive oxygen or nitrogen species (RONS) [56]. For AKI detection, the polyvinylpyrrolidone functionalized Pt NPs were used in vivo (BALB/c mice–glycerol-induced AKI), which resulted in significantly lower cellular damage induced by H_2O_2 as nanozymes. In addition, dual-modal photoacoustic (PA) and CT imaging, as well as ICP-MS analysis, confirmed the renal uptake of ultrasmall Pt NPs-PVP along with rapid excretion, lower toxicity, and fewer side effects. Nanoparticulates provide cellular protection against oxidative stress both in vitro and in vivo [57]. In another study, polyethylene glycol (PEG) modified Pt nanoworms (≥80 µg/mL) with high X-ray attenuation and photothermal efficiency killed 4T1 breast cancer cells in vitro. The

nanoworms formulation also successfully reduced the tumor load (4T1 breast cancer cell tumor model in BALB/c mice) assisted by near-infrared (NIR 1064 nm) laser exposure and radiation therapy in 14 days, as confirmed by PA and CT imaging, and as shown in Figure 4 (Figure 4A shows a TEM image of the Pt nanoworms, followed by the in vitro cytotoxicity of the formulation in 4T1 cells (Figure 4B). Figure 4C,D represents an increase in temperature in the presence of nanoworms in vitro and in 4T1-bearing mice when exposed to a laser source, respectively. The biodistribution of Pt nanoworms in an in vivo model is shown in Figure 4E, while Figure 4F,G represent the actual images of tumors extracted from the mouse model and changes in tumor volume with treatment in the different groups, respectively) [58]. Contrary to solid nanostructures, mesoporous Pt NPs delivered the doxorubicin (DOX) chemotherapy drug to DOX-resistant breast cancer cells (MCF-7/ADR) working as a dual theranostic agent for photothermal (PTT) and chemotherapy [59].
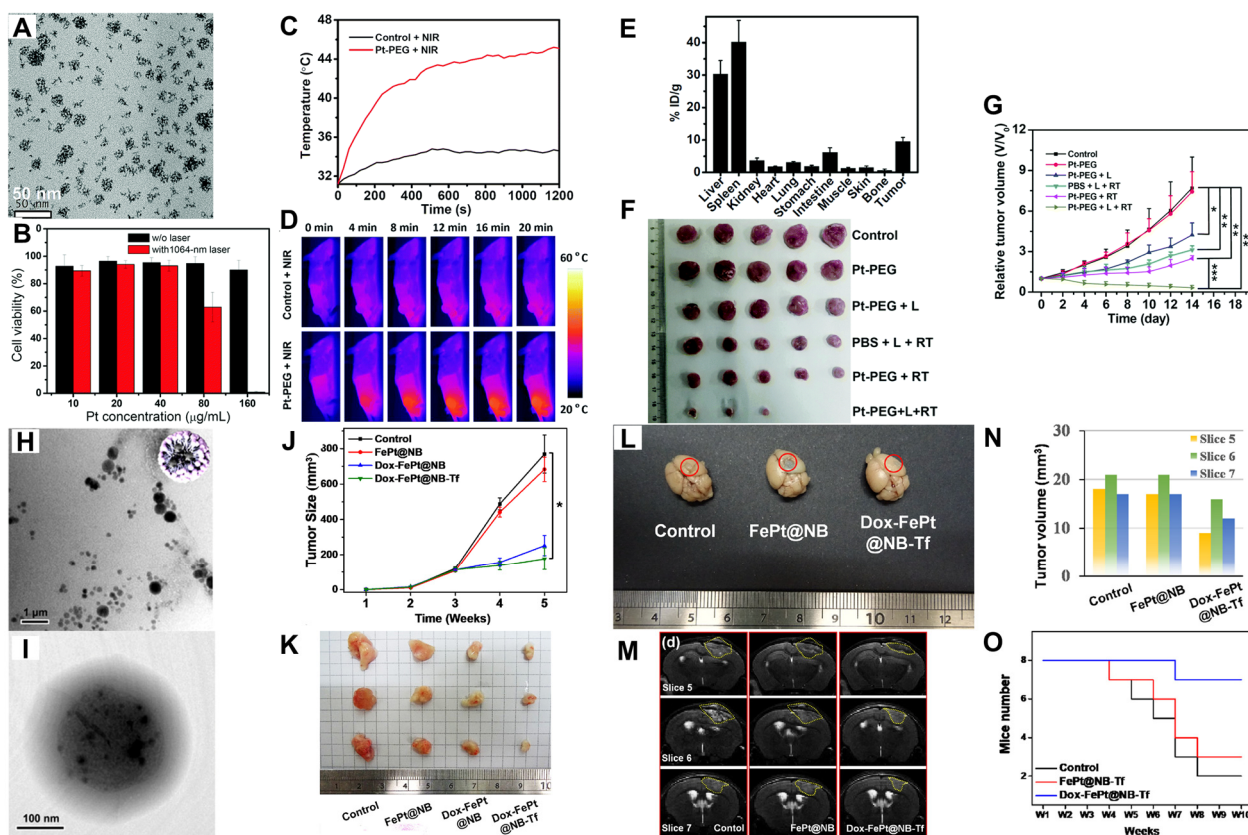

Figure 4. TEM image for Pt nanoworms shown in (**A**,**B**) represents the cell viability of 4T1 cells in vitro with photothermal and radiation therapy. For the in vivo model, (**C**) shows the heating curve with/without nanoworms when exposed to a NIR source and (**D**) represents the IR thermal image of control and Pt nanoworm-administered mice. (**E**) The in vivo biodistribution of Pt nanoworms in 4T1 tumor-bearing mice and (**F**) demonstrates the change in tumor size for 4T1 tumor-bearing mice with combination therapy, while (**G**) shows a change in tumor volume within different groups. The images were reused with permission from reference [58]. Copyright 2018, Royal Society of Chemistry. While in a hybrid Pt–Fe system for Dox delivery, (**H**,**I**) show the TEM image and high-resolution image of NPs. (**J**) Represents a change in GBM tumor size and (**K**) with actual GBM tumor photos for different groups. (**L**) Photos of GBM tumor size and (**M**) presents the MRI images with mouse brain in control, NPs, and drug-conjugated NPs (FePt-NB) groups. (**N**,**O**) demonstrates the change in tumor volume and the Kaplan–Meier survival curve. The images are reproduced with permission from reference [60]. (* $p < 0.05$, ** $p < 0.01$, and *** $p < 0.001$) Copyright 2021, American Chemical Society.

The theranostic potential of Pt NPs has also been investigated in conjugation with other types of metal NP. The NPs formulation harnessed the properties of gadolinium (Gd), a high-Z element that amplifies the therapeutic effect of radiation and is also known as a popular MRI contrast agent [61,62]. In an in vitro combination therapy model, ultra-small Pt NPs and Gd NPs (~3 nm) enhanced the efficiency of high-energy proton radiation therapy [63]. In addition, the hybrid iron–platinum (FePt) nanoparticles were exploited for the magnetic properties of iron (Fe) for magnetic field-guided targeting of hepatocellular carcinoma [64,65] and glioblastoma [60,66]. In two different studies by Ming-Hsien Chan et al., the 100 nm FePt NPs killed the HepG2 cells with DOX delivery [64] as well as Mahlava and SK-Hep1 hepatocellular carcinoma cells with mitoxantrone (MIT) [65] delivery in in vitro and in vivo models working as a chemotherapeutic and MRI diagnostic agent. The same group used a different approach involving PEGylated lipid nanobubbles for the magnetically guided delivery of DOX-conjugated FePt NPs. The formulation delivered the DOX drug across the blood–brain barrier (BBB) for a chemotherapeutic effect and also produced high-resolution imaging using a MRI for glioblastoma in an in vivo model. Figure 4H,I show TEM images of the Pt–Fe hybrid nanoformulations for DOX delivery to glioblastoma (GBM) tumor. Figure 4J,K represent the change in GBM size and actual photographs of the tumor with treatment, respectively. Figure 4L,M are the actual photographs and MRI images of the tumor located in the brain, respectively. Figure 4N,O represent the change in tumor volume and Kaplan–Meier survival in the three groups, respectively [60].

5. Palladium (Pd) Nanostructures

Palladium-based nanostructures are known for their unique optical properties, such as high stability and biocompatibility. In addition, high photothermal stability and high photothermal conversion efficiency make Pd-based NSs suitable for nanomedicine and diagnostic applications [67]. The relatively delayed interest in Pd NSs (NPs, nanosheets, porous/hollow NPs, and bi/multi-metallic nanocomposites) compared to Au and Ag has resulted in limited research studies. However, in the last decade, Pd-based NSs have been exploited for imaging modalities such as PA, SPECT, X-ray CT, and MR imaging. In addition, the focus has also been on therapeutic strategies using photothermal and photodynamic therapies independently or in combination with chemo, radio, hydrogen, and immune therapies.

Two independent studies used Pd NPs stabilized with chitosan and histidine to reduce the tumor size (MDA-MB-231 tumor and subcutaneous tumor, respectively) by killing the cancer cells using PTT when exposed to a near-infrared (NIR) laser [68,69]. Surface modification with molecules such as chitosan and PEG is known to improve stability and bioavailability. Furthermore, tagging the surface with targeting peptides like RGD/TAT, is known to significantly improve nanoparticle uptake in tumors [68,70,71]. Pristine Pd or bimetallic Pd–Au nanosheets or nanoplates modified with PEG/PVP not only support stability but also assist with anchoring other elements like Gd, F, ^{124}I, ^{177}Lu, and ^{64}Cu with the help of terminal groups on PEG/PVP [72–74]. Figure 5A,B show the schematic representation of Pd nanosheets and further modifications with gold and PEG, followed by the TEM image of PEGylated-Pd@Au nanosheets (C inset shows the colloidal suspension of nanosheets). Figure 4D shows the biodistribution of nanosheets in different organs harvested from a tumor-bearing mouse model. Figure 4E,F show IR thermal images of control and tumor-bearing mouse models and photoacoustic images of tumor sites, respectively. Figure 4G–I includes the change in tumor volume, the Kaplan–Meier survival curve, and actual photographs of mice with tumors after treatment, as shown in Figure 5 [73]. Based on the type of modification or active element, Pd-based nanostructures (NSs) have been utilized for PTT, photodynamic and radiotherapies of tumor theranostics as well as multi-modal imaging formulations using PA and PET [19,72,73,75–77]. Similarly, when conjugated with chemotherapy drugs, such as doxorubicin, these nanostructures successfully targeted breast and lung cancer cells in vitro [77] and delivered the DOX drug within the

tumor environment in vivo. The formulation, when assisted with combination therapies such as PTT reduced the 4T1 tumor volume in 18 days after intratumoral injection [78]. The prime focus of Pd-based nanostructures has been nanosheets, leaving the scope to explore different types of nanostructures for nanotheranostics, as well as different surface chemistries for the targeted and sustained delivery of therapeutic molecules.
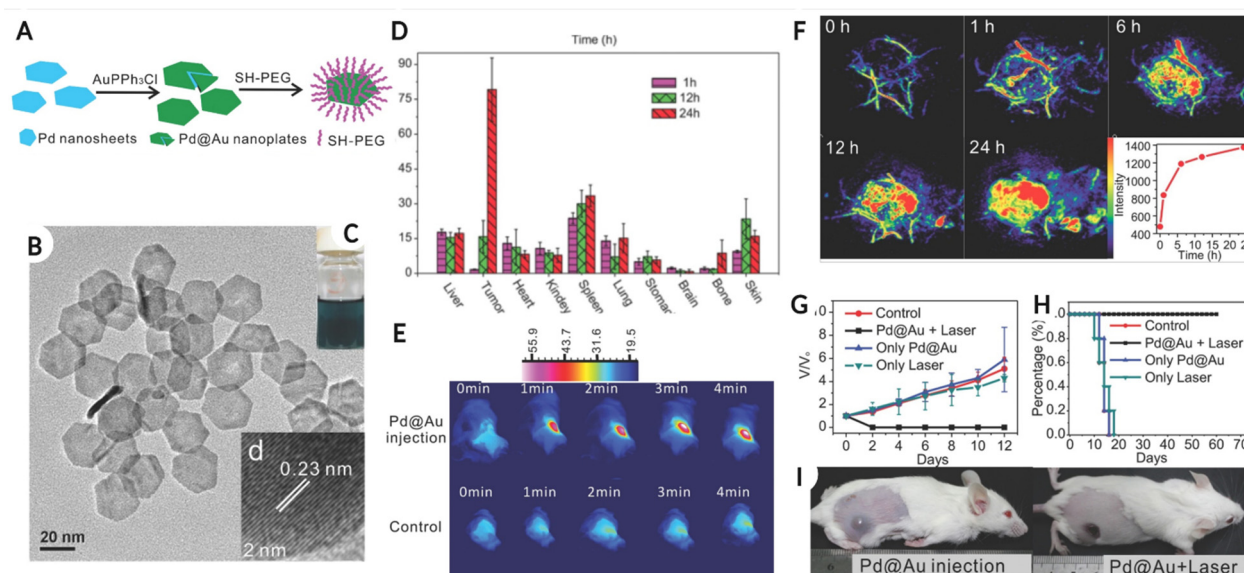

Figure 5. Palladium nanoplates as a theranostic agent. The schematic representation of Pd@Au nanoplate synthesis and TEM images shown in (**A**,**B**) with solution color in (**C**,**D**) demonstrate the quantitative analysis for biodistribution of Pd@Au nanoplates in different organs at various time points, (**d**) represents HRTEM image of a Pd@Au nanoplate flat lying on the TEM. (**E**) The IR thermal imaging of control and tumor mice injected with nanoplates while (**F**) presents the photoacoustic imaging of the tumor site at different time points. (**G**–**I**) show the change in tumor volume, Kaplan–Meier survival curve, and photos of mice after photothermal treatment, respectively, administered with Pd nanoplates. Images are reused with permission from reference [73]. Copyright 2014, Wiley.

6. Iridium (Ir) Nanostructures

Iridium (Ir)-based nanostructures have attracted interest because of their high catalytic activity for oxygen generation [79]. The high-Z element-based IrO_2 nanoparticles (40 nm) functionalized with bovine serum albumin (BSA, BSA-based biomineralization for the synthesis of NPs) were found to be anti-inflammatory and non-cytotoxic to L929 and HeLa cells. However, when exposed to NIR for PDT and PTT, the combination therapy resulted in more than 80% cell damage at 1.5 mM concentration in vitro. In addition, at the same concentration and therapy conditions, the formulation reduced tumor hypoxia, protected the healthy tissue from H_2O_2-induced inflammation, and depleted the U14 tumor in a mouse model in 14 days, as confirmed by thermal imaging [80]. While in a different study, BSA-IrO_2 nanoparticles encapsulated in biodegradable hollow mesoporous silica nanoparticles along with heat shock protein remained longer in the systemic circulation. The NP formulations also protected the major organs (liver, lung, kidney, spleen, and heart) from H_2O_2-assisted inflammation and heat damage, as well as accumulated in MDA-MB-231 tumor in in vivo. The study also confirmed a significant reduction in tumor size (scanned using CT and photoacoustic imaging) in mice exposed to PDT, PTT, and PDT-PTT combined, suggesting the potential for a nanotheranostic application [81]. Similar to the previous study, BSA-based biomineralized Ir and Mn nanoparticles modified with chlorin e6 (Ce6) facilitated X-ray CT and PA-guided PDT and PTT therapy as theranostic agents for a MDA-MB-231 tumor [82]. Figure 6A,B show the TEM images and absorbance graphs of IrO2 NPs modified with BSA-Ce6, respectively. Figure 4C shows the photothermal image of IrO2 NPs at different concentrations in Eppendorf when exposed to the laser,

while Figure 4D,E represent the oxygen generation using H2O2 and quantitative analysis of oxygen generation using RDPP fluorescence quenching assay, respectively. Figure 4F–H show traditional CT, MRI, and PA images of MDA-MB-231 tumors in an in vivo model injected with colloidal NPs. Figure 4I shows the fluorescence images of tumor-bearing mice injected with free Ce6 and BSA-Ce6-NPs, followed by biodistribution of NPs formulations in tumors and other organs at different time points. Figure 4K,L show the quantitative analysis of the change in tumor volume with treatment and the actual photograph of tumor size in different groups, respectively (Figure 6).
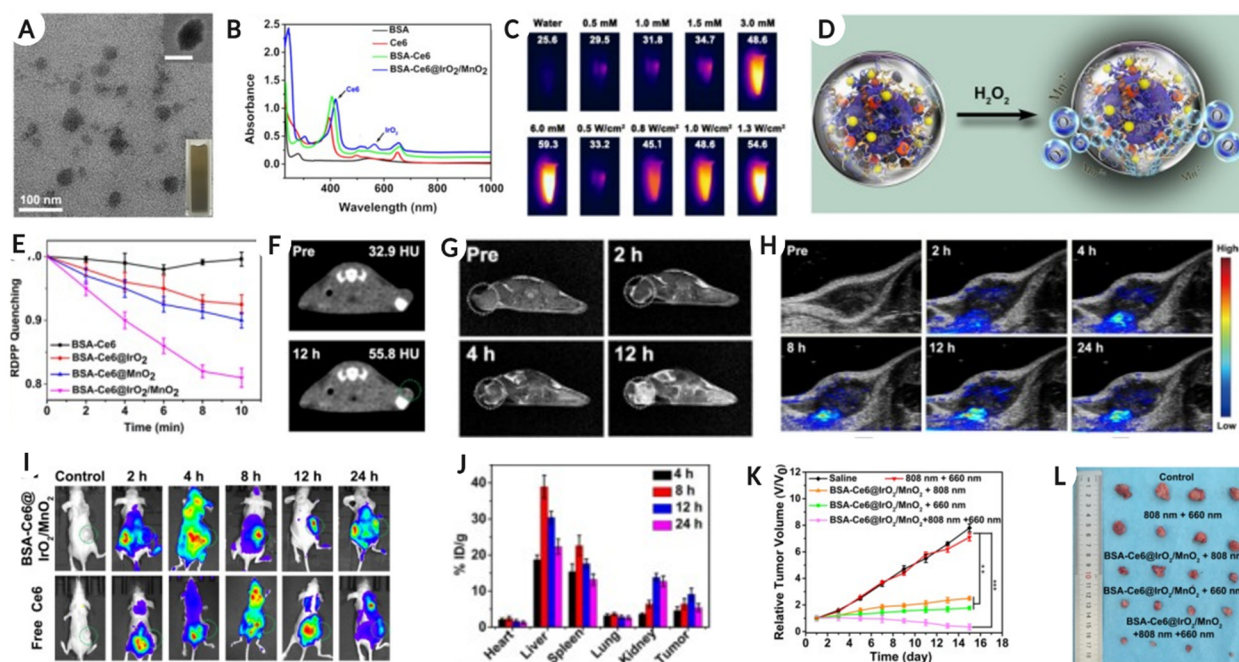

Figure 6. The TEM images and absorbance spectra for BSA-Ce6-modified hybrid iridium–manganese nanoparticles are shown in (**A**,**B**), respectively. (**C**) Represents the photothermal image of the Eppendorf with different concentrations of Ir: (**D**) is a schematic representation of oxygen generation with H_2O_2 utilization, and (**E**) shows the quantitative data for O_2 generation using RDPP fluorescence quenching assay. (**F**–**H**) represent the CT image, MRI image, and PA image of the MDA-MB-231 tumor in a mouse model, respectively, injected with BSA-Ce6 conjugated IrO_2/MnO_2 NPs. The fluorescence image of mice injected with free Ce6 and functionalized NPs shows the distribution (**I**) and the biodistribution of NPs in different organs in the mice model (**J**). The change in relative tumor volume is shown in (**K**), while (**L**) presents the photos of a tumor with the photothermal treatment. Images are reproduced with permission from reference [82]. (** $p < 0.01$, and *** $p < 0.001$) Copyright 2020, Ivyspring International Publisher.

In addition to solid Ir-based NSs, hollow mixed metallic (holmium and iridium) nanoparticles stabilized with PVP exhibited properties similar to those of pristine Ir-based NSs. These nanostructures showed the generation of singlet oxygen and high phosphorescence. The study also presented a proof of concept formulation to work as a multi-modality imaging agent for phosphorescence, ultrasound, and MR Imaging [83]. More recently, a complex Ir-based nanomicelle system was investigated by W. Abuduwaili et al. for chemo-photodynamic therapy against hepatocellular carcinoma (HCC). The self-assembled nanomicelle formulation composed of Ir complex with dpqx (O-phenylenediamine and Benzoyl) loaded with Sorafenib triggered the ROS-assisted PDT. PDT led to the inhibition of cell proliferation and cell death without causing harm to organs in vivo in an orthotopic xenograft HCC tumor model [84].

7. Rhodium (Rh), Osmium (Os), and Ruthenium (Ru) Nanostructures

Among noble metals, Rh, Os, and Ru have been actively explored for their catalytic and biosensing properties [85,86], but limited research has been conducted in the field of therapeutics and diagnostics in the last decade. PEGylated rhodium nanodots were utilized as nanozymes for free radical scavenging and PTT as well as for anti-tumor and anti-inflammatory effects for CT-26 colorectal carcinoma targeting (Figure 7A–C show TEM images of Rh NPs, absorbance, and oxygen generation at different concentrations. Figure 7D,E show the ROS staining (Figure 7D-1st row) and dead-live staining (Figure 7D-2nd row) for HUVECs and hemolysis analysis at different concentrations, respectively. Figure 7F shows the colon photographs and H&E, IL-4, TNF-α, and CD45 staining for the anti-inflammatory effect of Rh NPs. Figure 7G shows the PA image of the tumor site, and Figure 7H shows the IR thermal imaging of control and NP-injected mice at different time points, confirming the accumulation of NPs in the tumor. Figure 7I,J represent the actual tumor size and mouse photographs at the end of the study, with/without treatment, Figure 7). The nanodots did not accumulate in major organs like the heart, spleen, lung, and kidney until day 14. The study also showed a reduction in inflammatory markers at the colon cancer site, followed by the regeneration of colonic epithelial cells on day 9. The study also reported the elimination of tumor by day 16 in mice administered with PEGylated Rh nanodots [87]. In addition, there has been progress to develop metal–chemotherapy drug complexes based on rhodium, osmium, palladium, ruthenium, and iridium noble metals similar to cisplatin (Pt-based) [88].
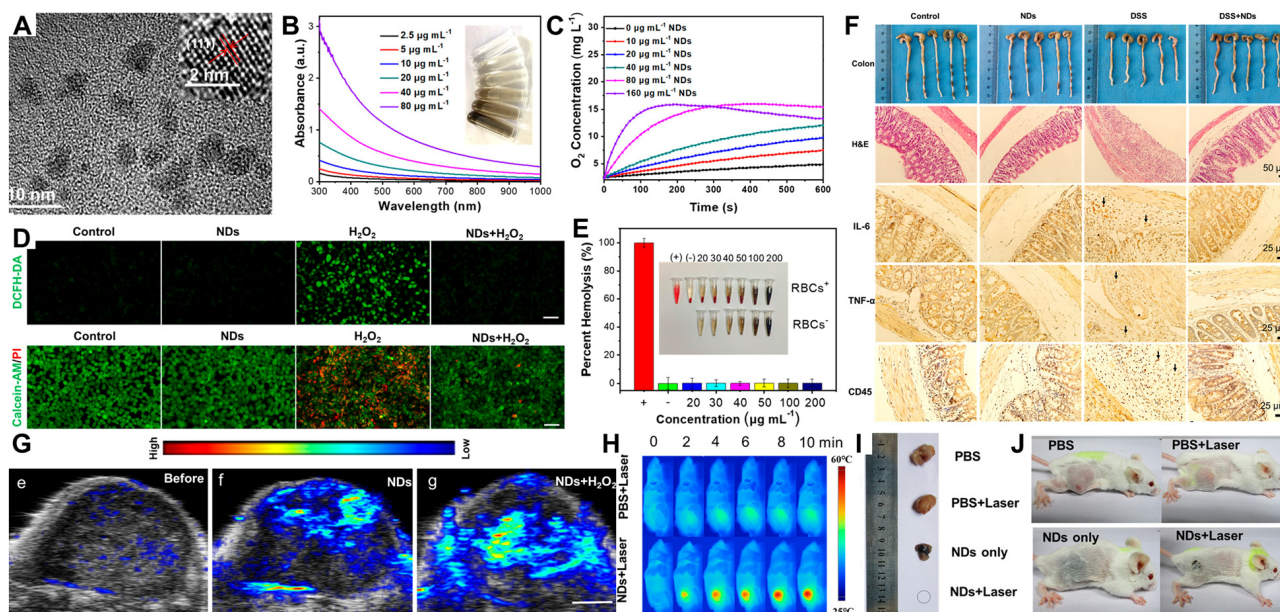

Figure 7. (**A**) TEM image of PEGylated Rh NPs; (**B**,**C**) the absorbance spectra for NPs and O_2 generation by NPs in the presence of H_2O_2, respectively. (**D**) First image row shows the ROS staining of HUVECs cells with DCFH-DA, and second row, shows Calcein and PI staining showing dead and alive HUVECs cells with H_2O_2 exposure and NPs treatment for cryoprotection and anti-inflammatory effect. (**E**) The hemolysis test at different NPs concentrations. (**F**) Photographs of colons extracted from various groups and histological images for H&E, IL-4, TNF-a, and CD45 staining for the same groups show anti-inflammatory treatment of colitis with NPs treatment. (**G**) Photoacoustic image of the tumor (no NPs), tumor with NPs, and tumor with NPs + H_2O_2. (**H**) IR thermal image of CT-26 tumor with temperature gradient with NPs and laser exposure. (**I**,**J**) Photographs of CT-26 tumor with treatment and actual image of mice with tumor at day 16. Images reused with permission from reference [87]. Copyright 2020, American Chemical Society.

Similar to Rh, there has been limited literature reporting the theranostic application of Osmium nanostructures since 2010. In an in vitro study, Osmium NSs (spherical, core–

shell, and nanorods) were found to be optothermal. The additional layer of silica not only improved the stability profile of NSs, but also increased the overall temperature and thermal conductivity within the NSs and system when exposed to a laser source [89]. More recently, Osmium–tellurium nanorods were explored for enzymatic activity and were found to exhibit excellent photothermal, photocatalytic, and photodynamic activity to act as a penta-modal treatment profile against hepatocellular carcinoma. The formulation reduced hypoxia by generating O_2, and reduced bone marrow and other organ toxicity by delivering the drug within the tumor. The mixed metal nanorod formulation also reduced immunotherapy resistance, and worked as a multi-modal therapy agent. The in vivo model survived the HCC after OsTe NSs administration and Chemo-PTT-PDT therapy for more than 45 days with reduced tumor volume (Figure 8, Figure 8A–C show the schematics of the OsTe nanorods, suspension color for Te NRs and OsTe NRs, and TEM images of OsTe nanostructures, respectively. Figure 8D is a schematic representation of different properties associated with OsTe NSs, while Figure 8E,F represent changes in temperature at different wavelengths and heating/cooling cycles when exposed to an 808 nm laser, respectively. Figure 8G,H show thermal imaging for control mice injected with PBS and mice injected with OsTe NSs, representing the accumulation of nanorods in the RIL-175 tumor and the change in tumor volume with therapy, respectively. Figure 8I shows the Kaplan–Meier survival curve for different groups) [90].
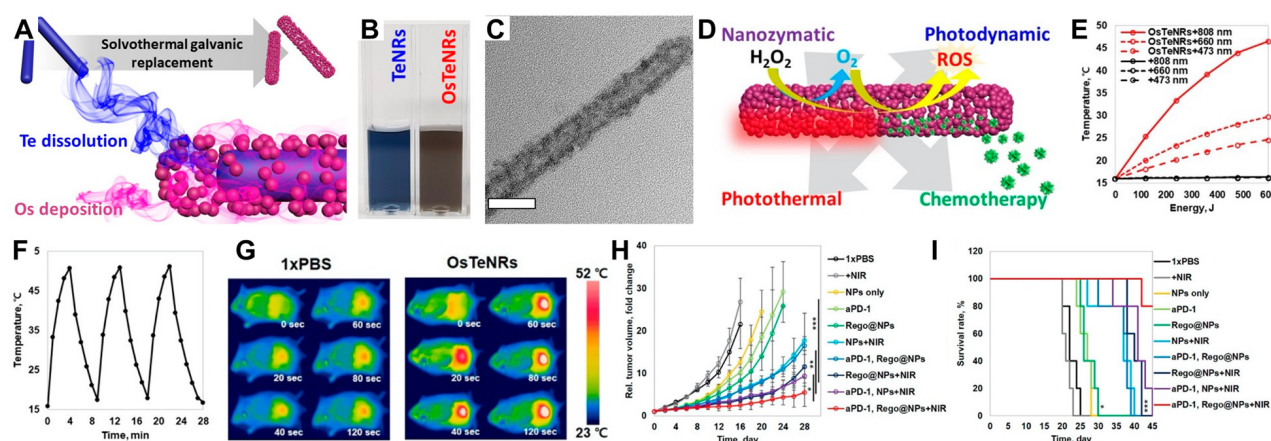

Figure 8. (**A**) Schematics showing the synthesis of OsTeNS by the solvothermal galvanic method, (**B**) the colloidal suspension color for TeNS and OsTeNS, and (**C**) the TEM image of OsTeNS. (**D**) A schematic representation of nanozymatic and photodynamic mechanism by Os-Te NS. (**E**,**F**) wavelength-dependent variability in temperature and heating/cooling cycle for OsTeNS when exposed to 808 nm laser, respectively. (**G**) Thermal imaging of RIL-175 tumor in mice injected with PBS and OsTeNS. (**H**,**I**) The change in relative tumor volume and Kaplan–Meier survival curve for tumor mice with NCTDI pentamodal therapy. Images reproduced with permission from reference [90]. Copyright 2021, American Chemical Society.

Similar to Cisplatin, which is a Pt-based chemotherapy agent, ruthenium (Ru)-based complexes (NAMI-A and KP109) have shown promising results as chemotherapy agents. Some of these formulations are already in clinical trials because of their properties, such as DNA structural probes and cellular imaging agents [91–93]. There have been studies involving the synthesis of Ru-based nanostructures, but relatively more focus has been placed on tagging silica and other nanoparticle types with Ru complexes for therapeutic and diagnostic applications. Different types of Ru complexes (tris-bipyridine–Ru (II), thiolated polypyridyl–Ru (II), antibacterial peptide–PEP, Tris(4,4'-dicarboxylic acid-2,2-bipyridyl) Ru (II) dichloride, tris(2.2'-bipyridine) Ru (II) hexafluorophosphatetriethylamine, tris(1.10-phenanthroline) ruthenium(II) complex (3P-Ru)) have been conjugated with silica, silver, mesoporous silica, selenium, polydopamine, metal–organic framework, lipid, pH-sensitive block polymer nanocapsules, and PLGA nanoparticles to employ for imaging (fluorescence,

photosensitizing, MRI, PAT,) and therapies (anti-bacterial, radiosensitizer, Chemo, PTT, PDT) [94–104].

Ru-based NSs such as nano-aggregates (2–3 nm nanoparticles–aggregating to form 40 nm bigger particles), nanosheets, ultra-small NPs, and mesoporous Ru-nanoparticles, have been employed for PTT, PDT, and photosensitizer therapies for cancer or tumor targeting. In such applications, surface chemistry plays a critical role in providing stability, active targeting, and selective uptake at the disease site. Such chemistries include immobilizing molecules like L-cysteine, BLZ-945 (CSF-1/CSF-1R inhibitor), transferrin-aptamer, anticancer molecule-[Ru (bpy) 2 (tip)]$^{2+}$, phenanthroline (Phen), and PEG on the surface of Ru-based nanostructures either to have a photothermal (localized elevation in temperature) effect when irradiated with a laser (808 nm) or generating localized reactive oxygen species to induce tumor cell apoptosis for therapeutic (PDT) and diagnostics applications in different cancer types [105–110]. Phenanthroline-modified Ru nanodots were synthesized for photothermal therapy, and the smaller size assisted with the renal clearance of NS. The non-toxic nano-formulation showed a concentration-dependent increase in temperature when exposed to the laser source and caused cytotoxicity, as reported for 4T1 cell types in vitro. However, in the in vivo T1 tumor mouse model, the 4T1 tumor was eradicated within 14 days with 808 nm laser-assisted photothermal therapy, and NSs were removed from the systemic circulation via renal clearance within 30 days. Figure 9A,B show the schematics of Ru nanodot synthesis and TEM images of nanodots/NSs, respectively. Figure 9C,D represent the changes in temperature at different powers and concentrations with time for nanodots, respectively. Figure 9E,F show 4T1, CT26, and HUVEC cell viability at different concentrations of nanodots and cell viability for 4T1 cells at different concentrations with and without laser exposure, respectively. Figure 9G,H show temperature gradient images of the tumor site using thermal imaging after nanodot injection, laser exposure, and change in temperature, respectively. Figure 9I–K show changes in tumor volume with and without nanodots as well as laser exposure, actual photographs of mice with tumors at the end of the study (mice exposed to Ru nanodots and laser–tumor eradicated), and biodistribution of nanodots in major organs at different time points, respectively, shown in Figure 9 [109].
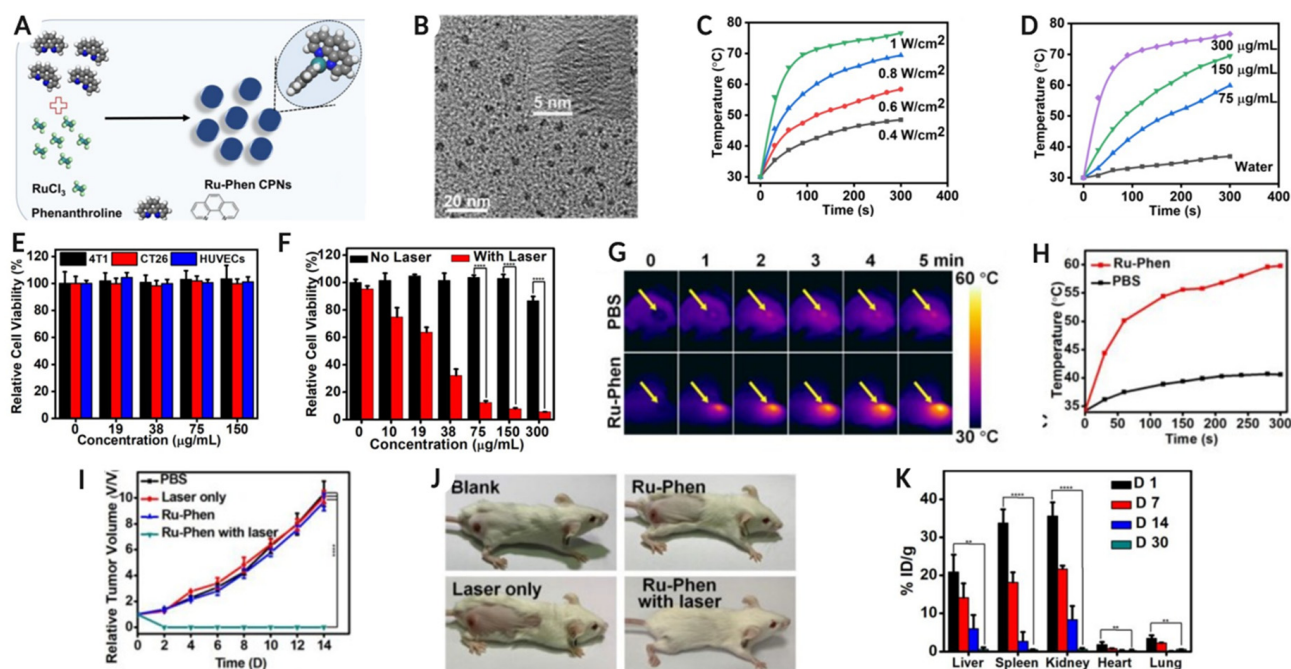

Figure 9. The synthesis schematics and TEM image of ultrasmall Ru nanodots are shown as (**A**,**B**), respectively. (**C**,**D**) The power and concentration-dependent increase in temperature in the presence of nanodots. (**E**) The nanodots were non-toxic to 4T1, CT26, and HUVECs cells up to 100 ug/mL (**F**)

but caused cytotoxicity with nanodot-treated cells (4T1) were exposed with an 808 nm laser. (**G**) IR thermal imaging of the 4T1 tumor mice model with temperature gradient profile during the first 5 min and (**H**) the measured temperature for 4T1 tumor-bearing mice with PBS or Ru-Phen nanodots up to 5 h. The relative change in tumor volume has been represented in image (**I**) and the optical photographs of tumor-bearing mice undergoing PTT treatment (**J**). The biodistribution profile of Ru-Phen nanodots quantified using ICP-MS is shown in the image (**K**) at different time points. Image reused with permission from reference [109]. Copyright 2019, Ivyspring International Publisher.

Generally, cancer treatment strategies, such as radiation, chemotherapy, and immunotherapy, work on cancer or tumors by delivering drugs or molecules to the tumor site. These molecules subsequently damage the key biomolecules like "DNA," creating a hostile environment by destroying major cell components or blocking the key pathways required for cancer cell function. These modes of action not only kill cancer cells but also interfere with healthy cell function, as suggested by the severe side effects and damage to the immune system. However, with active or passive noble metal nanoparticle delivery inside the tumor microenvironment followed by near-infrared laser exposure, localized heat can be generated, which disrupts cancer cell functions. In addition, with the delivery of photosensitizer agents, ROS generation and other anti-tumor immunity pathways are triggered by laser exposure. Both PTT and PDT create hostile environments that cause cancer cells to undergo necrosis, thereby killing cancer cells and reducing the tumor size [111].

8. Conclusions and Future Prospects

In the last decade, with advancements in the field of nanomaterials, several types of organic and inorganic nanostructures have emerged with promising potential over traditional therapeutic and surgical approaches for cancer treatment and diagnosis. The exponential growth in research on cancer biology and therapies has certainly improved the survival of cancer patients. However, the limitations of traditional treatment strategies highlight the need to develop novel materials to combat tumors at a molecular scale. The inclusion of chemical, engineering, and materials science in medicine for nanotheranostic applications can certainly provide chemical and topographical cues to cells for interaction. Such interactions, specifically with cancer cells, can lead to inhibiting cancer cell function, thereby killing cancer cells and tumor size reduction. These nanoparticle-based formulations have significantly improved the targeted delivery of therapeutic drugs within the tumor environment for anti-tumor potency but have also assisted in cancer imaging and diagnosis. With such formulations, we can also address challenges, such as tumor metastasis and multi-drug resistance, that directly impact patient survival.

In this review, we provide an overview of the applications of noble MNPs in cancer theranostic. Among inorganic nanostructures, noble metal nanoparticles/nanostructures are unique. Their ability to provide non-invasive or minimally invasive therapies, such as PTT, PDT, and PAT, can concurrently take advantage of chemo- or radiotherapy with immobilized or encapsulated active molecules on or within the NS. These NSs suspensions are known to be stable when exposed to a wide range of pH and physiological conditions. These noble metallic nanoparticles serve the purpose of real-time diagnosis tools using traditional computed tomography-based imaging techniques, as well as advanced thermal, acoustic, spectral photon counting, and dual photon counting imaging technologies. However, to date, the major research focus has been on gold and silver because of their easy-to-functionalize, stable, and biological properties. Other noble metallic nanoparticles like Pt and Pd have been amalgamated with gold for various biomedical applications, including cancer therapeutics. In contrast, Pd, Ir, Rh, Os, and Ru are still playing catch-up. The lack of exposure to these noble metals could be related to their availability and high cost. However, as the literature suggests, factors or properties, such as nanoparticle size, surface chemistry, cell type/disease type, and tumor location, can play a critical role in NPs uptake, screening the treatment and diagnostic regime. The discovery and application of metallic nanostructures composed of Ir, Rd, Os, Pd, and Ru (other than Ag, Ag, and Pt) can alter the future scope of nanotheranostic applications for cancer targeting. Furthermore,

Os (76), Ir (77), Pt (78), and Au (79) are also known to be high-Z elements. Among these elements, gold-based NS has been explored for novel spectral-photon counting or dual-photon counting imaging owing to its X-ray attenuation properties. However, as Os-, Ir-, and Pt-based NS belong to the same classification, these NSs should have similar properties and serve dual purposes for therapeutic and diagnostic applications. The amalgam of these applications is critical for futuristic personalized nanomedicine and nanotheranostic applications. The discovery and optimization of nanoformulations for cancer or any disease targeting and theranostic is complicated and time-consuming.

Despite the advancements in the field of nanomedicine and nanotheranostics, the research field is young. Very little is known about the long-term exposure of these NPs in humans and microbes, and their influence on ecological systems. Rigorous planning and experimental data are required to determine the biological and environmental safety of these nanomaterials. This review will be helpful to researchers working in the field of nanomedicine and nanotheranostics, highlighting the need to develop multifunctional and multi-modal imaging nanoformulations for diagnosis, delivery, and therapy.

Abbreviations

magnetic resonance imaging (MRI), positron emission tomography (PET), X-ray computed tomography (CT), photoacoustic tomography (PAT), magnetic resonance spectroscopy (MRS), single photon emission computed tomography (SPECT), spectral photon-counting CT (SPCCT), nanoparticles (NPs), metal nanoparticles (MNPs), nanostructures (NSs), nanocrystals (NCs), epidermal growth factor receptor (EGFR), insulin growth factor (IGF), polyethylene glycol modification (PEGylation) near infrared (NIR), gold nanorods (GNRs), high atomic number (high Z), reactive oxygen species (ROS), polyvinylpyrrolidone (PVP), photodynamic therapy (PDT), photothermal therapy (PTT).

References

1. Kievit, F.M.; Zhang, M. Cancer Nanotheranostics: Improving Imaging and Therapy by Targeted Delivery Across Biological Barriers. *Adv. Mater.* **2011**, *23*, H217–H247. [CrossRef]
2. Brindle, K. New approaches for imaging tumour responses to treatment. *Nat. Rev. Cancer* **2008**, *8*, 94–107. [CrossRef]
3. Cho, K.; Wang, X.; Nie, S.; Chen, Z.; Shin, D.M. Therapeutic Nanoparticles for Drug Delivery in Cancer. *Clin. Cancer Res.* **2008**, *14*, 1310–1316. [CrossRef]
4. Lim, E.-K.; Kim, T.; Paik, S.; Haam, S.; Huh, Y.-M.; Lee, K. Nanomaterials for Theranostics: Recent Advances and Future Challenges. *Chem. Rev.* **2015**, *115*, 327–394. [CrossRef]
5. Kim, H.; Kwak, G.; Kim, K.; Yoon, H.Y.; Kwon, I.C. Theranostic designs of biomaterials for precision medicine in cancer therapy. *Biomaterials* **2019**, *213*, 119207. [CrossRef] [PubMed]
6. Gilham, I. Theranostics—An Emerging Tool in drug Discovery and Commercialisation. *Drug Discov. World* **2002**, *6*, 24–32.
7. Wong, X.Y.; Sena-Torralba, A.; Álvarez-Diduk, R.; Muthoosamy, K.; Merkoçi, A. Nanomaterials for Nanotheranostics: Tuning Their Properties According to Disease Needs. *ACS Nano* **2020**, *14*, 2585–2627. [CrossRef]

8. Jagtap, P.; Sritharan, V.; Gupta, S. Nanotheranostic approaches for management of bloodstream bacterial infections. *Nanomed. Nanotechnol. Biol. Med.* **2017**, *13*, 329–341. [CrossRef] [PubMed]

9. Caldorera-Moore, M.E.; Liechty, W.B.; Peppas, N.A. Responsive Theranostic Systems: Integration of Diagnostic Imaging Agents and Responsive Controlled Release Drug Delivery Carriers. *Acc. Chem. Res.* **2011**, *44*, 1061–1070. [CrossRef] [PubMed]

10. Mura, S.; Couvreur, P. Nanotheranostics for personalized medicine. *Adv. Drug Deliv. Rev.* **2012**, *64*, 1394–1416. [CrossRef] [PubMed]

11. Roma-Rodrigues, C.; Pombo, I.; Raposo, L.; Pedrosa, P.; Fernandes, A.R.; Baptista, P.V. Nanotheranostics Targeting the Tumor Microenvironment. *Front. Bioeng. Biotechnol.* **2019**, *7*, 197. [CrossRef]

12. Thorek, D.L.J.; Chen, A.K.; Czupryna, J.; Tsourkas, A. Superparamagnetic Iron Oxide Nanoparticle Probes for Molecular Imaging. *Ann. Biomed. Eng.* **2006**, *34*, 23–38. [CrossRef] [PubMed]

13. Xie, J.; Chen, K.; Huang, J.; Lee, S.; Wang, J.; Gao, J.; Li, X.; Chen, X. PET/NIRF/MRI triple functional iron oxide nanoparticles. *Biomaterials* **2010**, *31*, 3016–3022. [CrossRef]

14. Thakor, A.S.; Gambhir, S.S. Nanooncology: The future of cancer diagnosis and therapy. *CA Cancer J. Clin.* **2013**, *63*, 395–418. [CrossRef]

15. Neuschmelting, V.; Harmsen, S.; Beziere, N.; Lockau, H.; Hsu, H.-T.; Huang, R.; Razansky, D.; Ntziachristos, V.; Kircher, M.F. Dual-Modality Surface-Enhanced Resonance Raman Scattering and Multispectral Optoacoustic Tomography Nanoparticle Approach for Brain Tumor Delineation. *Small* **2018**, *14*, 1800740. [CrossRef] [PubMed]

16. Vinci, G.; Rapa, M. Noble Metal Nanoparticles Applications: Recent Trends in Food Control. *Bioengineering* **2019**, *6*, 10. [CrossRef]

17. Liu, Y.; Yuan, H.; Fales, A.M.; Register, J.K.; Vo-Dinh, T. Multifunctional gold nanostars for molecular imaging and cancer therapy. *Front. Chem.* **2015**, *3*, 51. [CrossRef] [PubMed]

18. Liu, Y.; Yuan, H.; Kersey, F.; Register, J.; Parrott, M.; Vo-Dinh, T. Plasmonic Gold Nanostars for Multi-Modality Sensing and Diagnostics. *Sensors* **2015**, *15*, 3706–3720. [CrossRef] [PubMed]

19. Pang, B.; Zhao, Y.; Luehmann, H.; Yang, X.; Detering, L.; You, M.; Zhang, C.; Zhang, L.; Li, Z.-Y.; Ren, Q.; et al. 64 Cu-Doped PdCu@Au Tripods: A Multifunctional Nanomaterial for Positron Emission Tomography and Image-Guided Photothermal Cancer Treatment. *ACS Nano* **2016**, *10*, 3121–3131. [CrossRef] [PubMed]

20. Ravichandran, M.; Oza, G.; Velumani, S.; Ramirez, J.T.; Vera, A.; Leija, L. Design and evaluation of surface functionalized superparamagneto-plasmonic nanoparticles for cancer therapeutics. *Int. J. Pharm.* **2017**, *524*, 16–29. [CrossRef]

21. Conde, J.; Bao, C.; Cui, D.; Baptista, P.V.; Tian, F. Antibody–drug gold nanoantennas with Raman spectroscopic fingerprints for in vivo tumour theranostics. *J. Control. Release* **2014**, *183*, 87–93. [CrossRef] [PubMed]

22. Manivasagan, P.; Bharathiraja, S.; Santha Moorthy, M.; Oh, Y.-O.; Song, K.; Seo, H.; Oh, J. Anti-EGFR Antibody Conjugation of Fucoidan-Coated Gold Nanorods as Novel Photothermal Ablation Agents for Cancer Therapy. *ACS Appl. Mater. Interfaces* **2017**, *9*, 14633–14646. [CrossRef] [PubMed]

23. Li, C.; Mei, E.; Chen, C.; Li, Y.; Nugasur, B.; Hou, L.; Ding, X.; Hu, M.; Zhang, Y.; Su, Z.; et al. Gold-Nanobipyramid-Based Nanotheranostics for Dual-Modality Imaging-Guided Phototherapy. *ACS Appl. Mater. Interfaces* **2020**, *12*, 12541–12548. [CrossRef] [PubMed]

24. Baptista, P.; Fernandes, A.; Figueiredo, S.; Vinhas, R.; Cordeiro, M.; Carlos, F.; Mendo, S. Gold nanoparticle-based theranostics: Disease diagnostics and treatment using a single nanomaterial. *Nanobiosens. Dis. Diagn.* **2015**, *4*, 11–23. [CrossRef]

25. Dey, P.; Vaideanu, A.; Mosca, S.; Salimi, M.; Gardner, B.; Palombo, F.; Uchegbu, I.; Baumberg, J.; Schatzlein, A.; Matousek, P.; et al. Surface enhanced deep Raman detection of cancer tumour through 71 mm of heterogeneous tissue. *Nanotheranostics* **2022**, *6*, 337–349. [CrossRef]

26. Esmaeili, Y.; Khavani, M.; Bigham, A.; Sanati, A.; Bidram, E.; Shariati, L.; Zarrabi, A.; Jolfaie, N.A.; Rafienia, M. Mesoporous silica@chitosan@gold nanoparticles as "on/off" optical biosensor and pH-sensitive theranostic platform against cancer. *Int. J. Biol. Macromol.* **2022**, *202*, 241–255. [CrossRef]

27. Ashton, J.R.; Gottlin, E.B.; Patz, E.F.; West, J.L.; Badea, C.T. A comparative analysis of EGFR-targeting antibodies for gold nanoparticle CT imaging of lung cancer. *PLoS ONE* **2018**, *13*, e0206950. [CrossRef]

28. Cao, Y.; Wang, J.; Jiang, Q.-Y.; Hu, L.; Yu, Y.-J.; Yu, Y.-F.; Chen, F. A Gold Nanoparticle Bouquet held on plasma membrane: An ultrasensitive dark-field imaging approach for Cancer Cell Analysis. *Nanotheranostics* **2020**, *4*, 201–209. [CrossRef]

29. Yang, L.; Tseng, Y.-T.; Suo, G.; Chen, L.; Yu, J.; Chiu, W.-J.; Huang, C.-C.; Lin, C.-H. Photothermal Therapeutic Response of Cancer Cells to Aptamer–Gold Nanoparticle-Hybridized Graphene Oxide under NIR Illumination. *ACS Appl. Mater. Interfaces* **2015**, *7*, 5097–5106. [CrossRef]

30. Fales, A.M.; Yuan, H.; Vo-Dinh, T. Development of Hybrid Silver-Coated Gold Nanostars for Nonaggregated Surface-Enhanced Raman Scattering. *J. Phys. Chem. C* **2014**, *118*, 3708–3715. [CrossRef]

31. Fales, A.M.; Yuan, H.; Vo-Dinh, T. Cell-Penetrating Peptide Enhanced Intracellular Raman Imaging and Photodynamic Therapy. *Mol. Pharm.* **2013**, *10*, 2291–2298. [CrossRef] [PubMed]

32. Fales, A.M.; Yuan, H.; Vo-Dinh, T. Silica-Coated Gold Nanostars for Combined Surface-Enhanced Raman Scattering (SERS) Detection and Singlet-Oxygen Generation: A Potential Nanoplatform for Theranostics. *Langmuir* **2011**, *27*, 12186–12190. [CrossRef] [PubMed]

33. Li, M.; Wu, J.; Ma, M.; Feng, Z.; Mi, Z.; Rong, P.; Liu, D. Alkyne- and Nitrile-Anchored Gold Nanoparticles for Multiplex SERS Imaging of Biomarkers in Cancer Cells and Tissues. *Nanotheranostics* **2019**, *3*, 113–119. [CrossRef]

34. Zhang, S.; Gupta, S.; Fitzgerald, T.J.; Bogdanov, A.A. Dual radiosensitization and anti-STAT3 anti-proliferative strategy based on delivery of gold nanoparticle—Oligonucleotide nanoconstructs to head and neck cancer cells. *Nanotheranostics* **2018**, *2*, 1–11. [CrossRef]

35. Song, L.; Able, S.; Johnson, E.; Vallis, K.A. Accumulation of 111 In-Labelled EGF-Au-PEG Nanoparticles in EGFR-Positive Tumours is Enhanced by Coadministration of Targeting Ligand. *Nanotheranostics* **2017**, *1*, 232–243. [CrossRef] [PubMed]

36. Zhu, F.; Tan, G.; Jiang, Y.; Yu, Z.; Ren, F. Rational design of multi-stimuli-responsive gold nanorod–curcumin conjugates for chemo-photothermal synergistic cancer therapy. *Biomater. Sci.* **2018**, *6*, 2905–2917. [CrossRef] [PubMed]

37. Li, C.; Zhang, Y.; Li, Z.; Mei, E.; Lin, J.; Li, F.; Chen, C.; Qing, X.; Hou, L.; Xiong, L.; et al. Light-Responsive Biodegradable Nanorattles for Cancer Theranostics. *Adv. Mater.* **2018**, *30*, 1706150. [CrossRef]

38. Yang, W.; Wu, X.; Dou, Y.; Chang, J.; Xiang, C.; Yu, J.; Wang, J.; Wang, X.; Zhang, B. A human endogenous protein exerts multi-role biomimetic chemistry in synthesis of paramagnetic gold nanostructures for tumor bimodal imaging. *Biomaterials* **2018**, *161*, 256–269. [CrossRef]

39. Zhang, B.; Wang, J.; Yu, J.; Fang, X.; Wang, X.; Shi, D. Site-Specific Biomimetic Precision Chemistry of Bimodal Contrast Agent with Modular Peptides for Tumor-Targeted Imaging. *Bioconjug. Chem.* **2017**, *28*, 330–335. [CrossRef]

40. Sukumar, U.K.; Bose, R.J.C.; Malhotra, M.; Babikir, H.A.; Afjei, R.; Robinson, E.; Zeng, Y.; Chang, E.; Habte, F.; Sinclair, R.; et al. Intranasal delivery of targeted polyfunctional gold–iron oxide nanoparticles loaded with therapeutic microRNAs for combined theranostic multimodality imaging and presensitization of glioblastoma to temozolomide. *Biomaterials* **2019**, *218*, 119342. [CrossRef]

41. Yi, Y.; Kim, H.J.; Mi, P.; Zheng, M.; Takemoto, H.; Toh, K.; Kim, B.S.; Hayashi, K.; Naito, M.; Matsumoto, Y.; et al. Targeted systemic delivery of siRNA to cervical cancer model using cyclic RGD-installed unimer polyion complex-assembled gold nanoparticles. *J. Control. Release* **2016**, *244*, 247–256. [CrossRef]

42. Velasco-Aguirre, C.; Morales-Zavala, F.; Salas-Huenuleo, E.; Gallardo-Toledo, E.; Andonie, O.; Muñoz, L.; Rojas, X.; Acosta, G.; Sánchez-Navarro, M.; Giralt, E.; et al. Improving gold nanorod delivery to the central nervous system by conjugation to the shuttle Angiopep-2. *Nanomedicine* **2017**, *12*, 2503–2517. [CrossRef]

43. Lyu, M.; Chen, M.; Liu, L.; Zhu, D.; Wu, X.; Li, Y.; Rao, L.; Bao, Z. A platelet-mimicking theranostic platform for cancer interstitial brachytherapy. *Theranostics* **2021**, *11*, 7589–7599. [CrossRef] [PubMed]

44. Zhang, X.-F.; Liu, Z.-G.; Shen, W.; Gurunathan, S. Silver Nanoparticles: Synthesis, Characterization, Properties, Applications, and Therapeutic Approaches. *Int. J. Mol. Sci.* **2016**, *17*, 1534. [CrossRef] [PubMed]

45. Li, W.-R.; Xie, X.-B.; Shi, Q.-S.; Zeng, H.-Y.; OU-Yang, Y.-S.; Chen, Y.-B. Antibacterial activity and mechanism of silver nanoparticles on Escherichia coli. *Appl. Microbiol. Biotechnol.* **2010**, *85*, 1115–1122. [CrossRef] [PubMed]

46. Li, C.; Zhang, Y.; Wang, M.; Zhang, Y.; Chen, G.; Li, L.; Wu, D.; Wang, Q. In vivo real-time visualization of tissue blood flow and angiogenesis using Ag2S quantum dots in the NIR-II window. *Biomaterials* **2014**, *35*, 393–400. [CrossRef] [PubMed]

47. Chernousova, S.; Epple, M. Silver as Antibacterial Agent: Ion, Nanoparticle, and Metal. *Angew. Chem. Int. Ed.* **2013**, *52*, 1636–1653. [CrossRef]

48. Bhullar, S.K.; Ruzgar, D.G.; Fortunato, G.; Aneja, G.K.; Orhan, M.; Saber-Samandari, S.; Sadighi, M.; Ahadian, S.; Ramalingam, M. A Facile Method for Controlled Fabrication of Hybrid Silver Nanoparticle-Poly(-caprolactone) Fibrous Constructs with Antimicrobial Properties. *J. Nanosci. Nanotechnol.* **2019**, *19*, 6949–6955. [CrossRef]

49. Mukherjee, S.; Chowdhury, D.; Kotcherlakota, R.; Patra, S.; Vinothkumar, B.; Bhadra, M.P.; Sreedhar, B.; Patra, C.R. Potential Theranostics Application of Bio-Synthesized Silver Nanoparticles (4-in-1 System). *Theranostics* **2014**, *4*, 316–335. [CrossRef]

50. Srinivasan, S.; Bhardwaj, V.; Nagasetti, A.; Fernandez-Fernandez, A.; McGoron, A.J. Multifunctional Surface-Enhanced Raman Spectroscopy-Detectable Silver Nanoparticles for Combined Photodynamic Therapy and pH-Triggered Chemotherapy. *J. Biomed. Nanotechnol.* **2016**, *12*, 2202–2219. [CrossRef]

51. Ahmed B, S.; Baijal, G.; Somashekar, R.; Iyer, S.; Nayak, V. Comparative study of one pot synthesis of PEGylated gold and silver nanoparticles for imaging and radiosensitization of oral cancers. *Radiat. Phys. Chem.* **2022**, *194*, 109990. [CrossRef]

52. Dutta, D.; Sahoo, A.K.; Chattopadhyay, A.; Ghosh, S.S. Bimetallic silver nanoparticle–gold nanocluster embedded composite nanoparticles for cancer theranostics. *J. Mater. Chem. B* **2016**, *4*, 793–800. [CrossRef]

53. Grabowska-Jadach, I.; Kalinowska, D.; Drozd, M.; Pietrzak, M. Synthesis, characterization and application of plasmonic hollow gold nanoshells in a photothermal therapy—New particles for theranostics. *Biomed. Pharmacother.* **2019**, *111*, 1147–1155. [CrossRef] [PubMed]

54. Choi, G.; Kim, E.; Park, E.; Lee, J.H. A cost-effective chemiluminescent biosensor capable of early diagnosing cancer using a combination of magnetic beads and platinum nanoparticles. *Talanta* **2017**, *162*, 38–45. [CrossRef] [PubMed]

55. Yu, H.; Yu, J.; Li, L.; Zhang, Y.; Xin, S.; Ni, X.; Sun, Y.; Song, K. Recent Progress of the Practical Applications of the Platinum Nanoparticle-Based Electrochemistry Biosensors. *Front. Chem.* **2021**, *9*, 677876. [CrossRef]

56. Heemskerk, S.; Masereeuw, R.; Russel, F.G.M.; Pickkers, P. Selective iNOS inhibition for the treatment of sepsis-induced acute kidney injury. *Nat. Rev. Nephrol.* **2009**, *5*, 629–640. [CrossRef]

57. Zhang, D.-Y.; Liu, H.; Younis, M.R.; Lei, S.; Yang, C.; Lin, J.; Qu, J.; Huang, P. Ultrasmall platinum nanozymes as broad-spectrum antioxidants for theranostic application in acute kidney injury. *Chem. Eng. J.* **2021**, *409*, 127371. [CrossRef]

58. Ma, Q.; Cheng, L.; Gong, F.; Dong, Z.; Liang, C.; Wang, M.; Feng, L.; Li, Y.; Liu, Z.; Li, C.; et al. Platinum nanoworms for imaging-guided combined cancer therapy in the second near-infrared window. *J. Mater. Chem. B* **2018**, *6*, 5069–5079. [CrossRef]

59. Fu, B.; Dang, M.; Tao, J.; Li, Y.; Tang, Y. Mesoporous platinum nanoparticle-based nanoplatforms for combined chemo-photothermal breast cancer therapy. *J. Colloid Interface Sci.* **2020**, *570*, 197–204. [CrossRef]

60. Chan, M.-H.; Chen, W.; Li, C.-H.; Fang, C.-Y.; Chang, Y.-C.; Wei, D.-H.; Liu, R.-S.; Hsiao, M. An Advanced In Situ Magnetic Resonance Imaging and Ultrasonic Theranostics Nanocomposite Platform: Crossing the Blood–Brain Barrier and Improving the Suppression of Glioblastoma Using Iron-Platinum Nanoparticles in Nanobubbles. *ACS Appl. Mater. Interfaces* **2021**, *13*, 26759–26769. [CrossRef]

61. Sancey, L.; Lux, F.; Kotb, S.; Roux, S.; Dufort, S.; Bianchi, A.; Crémillieux, Y.; Fries, P.; Coll, J.-L.; Rodriguez-Lafrasse, C.; et al. The use of theranostic gadolinium-based nanoprobes to improve radiotherapy efficacy. *Br. J. Radiol.* **2014**, *87*, 20140134. [CrossRef]

62. Štefančíková, L.; Porcel, E.; Eustache, P.; Li, S.; Salado, D.; Marco, S.; Guerquin-Kern, J.-L.; Réfrégiers, M.; Tillement, O.; Lux, F.; et al. Cell localisation of gadolinium-based nanoparticles and related radiosensitising efficacy in glioblastoma cells. *Cancer Nanotechnol.* **2014**, *5*, 6. [CrossRef] [PubMed]

63. Schlatholter, T.; Lacombe, S.; Eustache, P.; Porcel, E.; Salado, D.; Stefancikova, L.; Tillement, O.; Lux, F.; Mowat, P.; van Goethem, M.-J.; et al. Improving proton therapy by metal-containing nanoparticles: Nanoscale insights. *Int. J. Nanomed.* **2016**, *11*, 1549. [CrossRef] [PubMed]

64. Chan, M.-H.; Hsieh, M.-R.; Liu, R.-S.; Wei, D.-H.; Hsiao, M. Magnetically Guided Theranostics: Optimizing Magnetic Resonance Imaging with Sandwich-Like Kaolinite-Based Iron/Platinum Nanoparticles for Magnetic Fluid Hyperthermia and Chemotherapy. *Chem. Mater.* **2020**, *32*, 697–708. [CrossRef]

65. Chan, M.-H.; Lu, C.-N.; Chung, Y.-L.; Chang, Y.-C.; Li, C.-H.; Chen, C.-L.; Wei, D.-H.; Hsiao, M. Magnetically guided theranostics: Montmorillonite-based iron/platinum nanoparticles for enhancing in situ MRI contrast and hepatocellular carcinoma treatment. *J. Nanobiotechnol.* **2021**, *19*, 308. [CrossRef]

66. Chen, W.; Chan, M.-H.; Hsiao, M. Magnetic and Ultrasonic Guidance of Iron–Platinum Nanoparticles Encapsulated in Multifunctional Lipid Bubbles for Conquering the Blood-Brain Barrier with Improved Theranostics. *FASEB J.* **2020**, *34*, 1. [CrossRef]

67. Liu, Y.; Li, J.; Chen, M.; Chen, X.; Zheng, N. Palladium-based nanomaterials for cancer imaging and therapy. *Theranostics* **2020**, *10*, 10057–10074. [CrossRef] [PubMed]

68. Bharathiraja, S.; Bui, N.Q.; Manivasagan, P.; Moorthy, M.S.; Mondal, S.; Seo, H.; Phuoc, N.T.; Vy Phan, T.T.; Kim, H.; Lee, K.D.; et al. Multimodal tumor-homing chitosan oligosaccharide-coated biocompatible palladium nanoparticles for photo-based imaging and therapy. *Sci. Rep.* **2018**, *8*, 500. [CrossRef] [PubMed]

69. Rubio-Ruiz, B.; Pérez-López, A.M.; Bray, T.L.; Lee, M.; Serrels, A.; Prieto, M.; Arruebo, M.; Carragher, N.O.; Sebastián, V.; Unciti-Broceta, A. High-Precision Photothermal Ablation Using Biocompatible Palladium Nanoparticles and Laser Scanning Microscopy. *ACS Appl. Mater. Interfaces* **2018**, *10*, 3341–3348. [CrossRef]

70. Shi, S.; Chen, X.; Wei, J.; Huang, Y.; Weng, J.; Zheng, N. Platinum(IV) prodrug conjugated Pd@Au nanoplates for chemotherapy and photothermal therapy. *Nanoscale* **2016**, *8*, 5706–5713. [CrossRef]

71. Gao, G.; Jiang, Y.-W.; Jia, H.-R.; Sun, W.; Guo, Y.; Yu, X.-W.; Liu, X.; Wu, F.-G. From perinuclear to intranuclear localization: A cell-penetrating peptide modification strategy to modulate cancer cell migration under mild laser irradiation and improve photothermal therapeutic performance. *Biomaterials* **2019**, *223*, 119443. [CrossRef] [PubMed]

72. Li, S.; Gu, K.; Wang, H.; Xu, B.; Li, H.; Shi, X.; Huang, Z.; Liu, H. Degradable Holey Palladium Nanosheets with Highly Active 1D Nanoholes for Synergetic Phototherapy of Hypoxic Tumors. *J. Am. Chem. Soc.* **2020**, *142*, 5649–5656. [CrossRef] [PubMed]

73. Chen, M.; Tang, S.; Guo, Z.; Wang, X.; Mo, S.; Huang, X.; Liu, G.; Zheng, N. Core-Shell Pd@Au Nanoplates as Theranostic Agents for In-Vivo Photoacoustic Imaging, CT Imaging, and Photothermal Therapy. *Adv. Mater.* **2014**, *26*, 8210–8216. [CrossRef] [PubMed]

74. Guo, Z.; Chen, M.; Peng, C.; Mo, S.; Shi, C.; Fu, G.; Wen, X.; Zhuang, R.; Su, X.; Liu, T.; et al. pH-sensitive radiolabeled and superfluorinated ultra-small palladium nanosheet as a high-performance multimodal platform for tumor theranostics. *Biomaterials* **2018**, *179*, 134–143. [CrossRef] [PubMed]

75. Zhu, X.; Chi, X.; Chen, J.; Wang, L.; Wang, X.; Chen, Z.; Gao, J. Real-Time Monitoring in Vivo Behaviors of Theranostic Nanoparticles by Contrast-Enhanced T 1 Imaging. *Anal. Chem.* **2015**, *87*, 8941–8948. [CrossRef]

76. Zhang, Y.; Lv, F.; Cheng, Y.; Yuan, Z.; Yang, F.; Liu, C.; Cao, Y.; Zhang, K.; Lu, H.; Zada, S.; et al. Pd@Au Bimetallic Nanoplates Decorated Mesoporous MnO_2 for Synergistic Nucleus-Targeted NIR-II Photothermal and Hypoxia-Relieved Photodynamic Therapy. *Adv. Healthc. Mater.* **2020**, *9*, 1901528. [CrossRef] [PubMed]

77. Oladipo, A.O.; Unuofin, J.O.; Iku, S.I.I.; Nkambule, T.T.I.; Mamba, B.B.; Msagati, T.A.M. Bimetallic Au@Pd nanodendrite system incorporating multimodal intracellular imaging for improved doxorubicin antitumor efficiency. *Int. J. Pharm.* **2021**, *602*, 120661. [CrossRef] [PubMed]

78. Zhu, W.; Chen, M.; Liu, Y.; Tian, Y.; Song, Z.; Song, G.; Zhang, X. A dual factor activated metal–organic framework hybrid nanoplatform for photoacoustic imaging and synergetic photo-chemotherapy. *Nanoscale* **2019**, *11*, 20630–20637. [CrossRef] [PubMed]

79. Bezbaruah, A.N.; Zhang, T.C. Fabrication of Anodically Electrodeposited Iridium Oxide Film pH Microelectrodes for Microenvironmental Studies. *Anal. Chem.* **2002**, *74*, 5726–5733. [CrossRef]

80. Zhen, W.; Liu, Y.; Lin, L.; Bai, J.; Jia, X.; Tian, H.; Jiang, X. BSA-IrO_2: Catalase-like Nanoparticles with High Photothermal Conversion Efficiency and a High X-ray Absorption Coefficient for Anti-inflammation and Antitumor Theranostics. *Angew. Chem. Int. Ed.* **2018**, *57*, 10309–10313. [CrossRef]

81. Wu, J.; Niu, S.; Bremner, D.H.; Nie, W.; Fu, Z.; Li, D.; Zhu, L. A Tumor Microenvironment-Responsive Biodegradable Mesoporous Nanosystem for Anti-Inflammation and Cancer Theranostics. *Adv. Healthc. Mater.* **2020**, *9*, 1901307. [CrossRef] [PubMed]

82. Wu, J.; Williams, G.R.; Niu, S.; Yang, Y.; Li, Y.; Zhang, X.; Zhu, L.-M. Biomineralized Bimetallic Oxide Nanotheranostics for Multimodal Imaging-Guided Combination Therapy. *Theranostics* **2020**, *10*, 841–855. [CrossRef] [PubMed]

83. Zhai, T.; Wang, C.; Cui, L.; Du, J.; Zhou, Z.; Yang, H.; Yang, S. Hollow Bimetallic Complex Nanoparticles for Trimodality Imaging and Photodynamic Therapy In Vivo. *ACS Appl. Mater. Interfaces* **2020**, *12*, 37470–37476. [CrossRef] [PubMed]

84. Abuduwaili, W.; Wang, X.; Huang, A.T.; Sun, J.L.; Xu, R.C.; Zhang, G.C.; Liu, Z.Y.; Wang, F.; Zhu, C.F.; Liu, T.T.; et al. Iridium Complex-Loaded Sorafenib Nanocomposites for Synergistic Chemo-photodynamic Therapy of Hepatocellular Carcinoma. *ACS Appl. Mater. Interfaces* **2022**, *14*, 37356–37368. [CrossRef]

85. Doria, G.; Conde, J.; Veigas, B.; Giestas, L.; Almeida, C.; Assunção, M.; Rosa, J.; Baptista, P.V. Noble Metal Nanoparticles for Biosensing Applications. *Sensors* **2012**, *12*, 1657–1687. [CrossRef] [PubMed]

86. Rodrigues, T.S.; da Silva, A.G.M.; Camargo, P.H.C. Nanocatalysis by noble metal nanoparticles: Controlled synthesis for the optimization and understanding of activities. *J. Mater. Chem. A* **2019**, *7*, 5857–5874. [CrossRef]

87. Miao, Z.; Jiang, S.; Ding, M.; Sun, S.; Ma, Y.; Younis, M.R.; He, G.; Wang, J.; Lin, J.; Cao, Z.; et al. Ultrasmall Rhodium Nanozyme with RONS Scavenging and Photothermal Activities for Anti-Inflammation and Antitumor Theranostics of Colon Diseases. *Nano Lett.* **2020**, *20*, 3079–3089. [CrossRef] [PubMed]

88. Ferraro, M.G.; Piccolo, M.; Misso, G.; Santamaria, R.; Irace, C. Bioactivity and Development of Small Non-Platinum Metal-Based Chemotherapeutics. *Pharmaceutics* **2022**, *14*, 954. [CrossRef]

89. Heidari, A.; Schmitt, K.; Henderson, M.; Besana, E. Drug delivery systems (DDSs) of osmium nanoparticles on human gum cancer cells, tissues and tumors treatment under synchrotron radiation. *Dent. Oral Maxillofac. Res.* **2019**, *5*, 1–18. [CrossRef]

90. Kang, S.; Gil, Y.-G.; Yim, G.; Min, D.-H.; Jang, H. Osmium–Tellurium Nanozymes for Pentamodal Combinatorial Cancer Therapy. *ACS Appl. Mater. Interfaces* **2021**, *13*, 44124–44135. [CrossRef]

91. Ferraro, M.G.; Piccolo, M.; Misso, G.; Maione, F.; Montesarchio, D.; Caraglia, M.; Paduano, L.; Santamaria, R.; Irace, C. Breast Cancer Chemotherapeutic Options: A General Overview on the Preclinical Validation of a Multi-Target Ruthenium(III) Complex Lodged in Nucleolipid Nanosystems. *Cells* **2020**, *9*, 1412. [CrossRef] [PubMed]

92. Liu, J.; Lai, H.; Xiong, Z.; Chen, B.; Chen, T. Functionalization and cancer-targeting design of ruthenium complexes for precise cancer therapy. *Chem. Commun.* **2019**, *55*, 9904–9914. [CrossRef] [PubMed]

93. Li, C.; Xu, Y.; Tu, L.; Choi, M.; Fan, Y.; Chen, X.; Sessler, J.L.; Kim, J.S.; Sun, Y. Rationally designed Ru (II)-metallacycle chemo-phototheranostic that emits beyond 1000 nm. *Chem. Sci.* **2022**, *13*, 6541–6549. [CrossRef] [PubMed]

94. Lechevallier, S.; Mauricot, R.; Gros-Dagnac, H.; Chevreux, S.; Lemercier, G.; Phonesouk, E.; Golzio, M.; Verelst, M. Silica-Based Nanoparticles as Bifunctional and Bimodal Imaging Contrast Agents. *Chempluschem* **2017**, *82*, 770–777. [CrossRef] [PubMed]

95. Wumaier, M.; Yao, T.-M.; Hu, X.-C.; Hu, Z.-A.; Shi, S. Luminescent Ru (II)-thiol modified silver nanoparticles for lysosome targeted theranostics. *Dalt. Trans.* **2019**, *48*, 10393–10397. [CrossRef] [PubMed]

96. Frasconi, M.; Liu, Z.; Lei, J.; Wu, Y.; Strekalova, E.; Malin, D.; Ambrogio, M.W.; Chen, X.; Botros, Y.Y.; Cryns, V.L.; et al. Photoexpulsion of Surface-Grafted Ruthenium Complexes and Subsequent Release of Cytotoxic Cargos to Cancer Cells from Mesoporous Silica Nanoparticles. *J. Am. Chem. Soc.* **2013**, *135*, 11603–11613. [CrossRef] [PubMed]

97. Huang, N.; Chen, X.; Zhu, X.; Xu, M.; Liu, J. Ruthenium complexes/polypeptide self-assembled nanoparticles for identification of bacterial infection and targeted antibacterial research. *Biomaterials* **2017**, *141*, 296–313. [CrossRef]

98. Zhang, M.; Wang, L.; Liu, H.; Wang, Z.; Feng, W.; Jin, H.; Liu, S.; Lan, S.; Liu, Y.; Zhang, H. Copper Ion and Ruthenium Complex Codoped Polydopamine Nanoparticles for Magnetic Resonance/Photoacoustic Tomography Imaging-Guided Photody- namic/Photothermal Dual-Mode Therapy. *ACS Appl. Bio Mater.* **2022**, *5*, 2365–2376. [CrossRef]

99. Chen, R.; Zhang, J.; Chelora, J.; Xiong, Y.; Kershaw, S.V.; Li, K.F.; Lo, P.-K.; Cheah, K.W.; Rogach, A.L.; Zapien, J.A.; et al. Ruthenium(II) Complex Incorporated UiO-67 Metal–Organic Framework Nanoparticles for Enhanced Two-Photon Fluorescence Imaging and Photodynamic Cancer Therapy. *ACS Appl. Mater. Interfaces* **2017**, *9*, 5699–5708. [CrossRef]

100. Wang, Q.; Fu, C.; Zhao, Z.; Fu, A. Targeted Theranostic of Cryptococcal Encephalitis by a Novel Polypyridyl Ruthenium Complex. *Mol. Pharm.* **2020**, *17*, 145–154. [CrossRef]

101. Chen, L.; Fu, C.; Deng, Y.; Wu, W.; Fu, A. A pH-Sensitive Nanocarrier for Tumor Targeting. *Pharm. Res.* **2016**, *33*, 2989–2998. [CrossRef] [PubMed]

102. Gill, M.R.; Menon, J.U.; Jarman, P.J.; Owen, J.; Skaripa-Koukelli, I.; Able, S.; Thomas, J.A.; Carlisle, R.; Vallis, K.A. 111 In-labelled polymeric nanoparticles incorporating a ruthenium-based radiosensitizer for EGFR-targeted combination therapy in oesophageal cancer cells. *Nanoscale* **2018**, *10*, 10596–10608. [CrossRef] [PubMed]

103. Hu, X.; Lu, Y.; Dong, C.; Zhao, W.; Wu, X.; Zhou, L.; Chen, L.; Yao, T.; Shi, S. A Ru II Polypyridyl Alkyne Complex Based Metal–Organic Frameworks for Combined Photodynamic/Photothermal/Chemotherapy. *Chem.–Eur. J.* **2020**, *26*, 1668–1675. [CrossRef] [PubMed]

104. Zhao, Y.; Ye, Y.; Zhou, X.; Chen, J.; Jin, Y.; Hanson, A.; Zhao, J.X.; Wu, M. Photosensitive Fluorescent Dye Contributes to Phototoxicity and Inflammatory Responses of Dye-doped Silica Nanoparticles in Cells and Mice. *Theranostics* **2014**, *4*, 445–459. [CrossRef] [PubMed]

105. Wang, W.-L.; Guo, Z.; Lu, Y.; Shen, X.-C.; Chen, T.; Huang, R.-T.; Zhou, B.; Wen, C.; Liang, H.; Jiang, B.-P. Receptor-Mediated and Tumor-Microenvironment Combination-Responsive Ru Nanoaggregates for Enhanced Cancer Phototheranostics. *ACS Appl. Mater. Interfaces* **2019**, *11*, 17294–17305. [CrossRef]

106. Zhu, X.; Zhou, H.; Liu, Y.; Wen, Y.; Wei, C.; Yu, Q.; Liu, J. Transferrin/aptamer conjugated mesoporous ruthenium nanosystem for redox-controlled and targeted chemo-photodynamic therapy of glioma. *Acta Biomater.* **2018**, *82*, 143–157. [CrossRef]

107. Liu, Y.; Wen, Y.; Chen, X.; Zhu, X.; Yu, Q.; Gong, Y.; Yuan, G.; Liu, J.; Qin, X. Inflammation-responsive functional Ru nanoparticles combining a tumor-associated macrophage repolarization strategy with phototherapy for colorectal cancer therapy. *J. Mater. Chem. B* **2019**, *7*, 6210–6223. [CrossRef]

108. Chen, G.; Xu, M.; Zhao, S.; Sun, J.; Yu, Q.; Liu, J. Pompon-like RuNPs-Based Theranostic Nanocarrier System with Stable Photoacoustic Imaging Characteristic for Accurate Tumor Detection and Efficient Phototherapy Guidance. *ACS Appl. Mater. Interfaces* **2017**, *9*, 33645–33659. [CrossRef]

109. Zhang, R.; Fan, X.; Meng, Z.; Lin, H.; Jin, Q.; Gong, F.; Dong, Z.; Li, Y.; Chen, Q.; Liu, Z.; et al. Renal Clearable Ru-based Coordination Polymer Nanodots for Photoacoustic Imaging Guided Cancer Therapy. *Theranostics* **2019**, *9*, 8266–8276. [CrossRef]

110. Chen, Z.; Zeng, Y.; Chen, N.; Zhang, M.; Wang, Y.; Pan, Z.; Yuan, J.; Ye, Z.; Li, X.; Bian, W.; et al. A Facile and Universal Method for Preparing Polyethylene Glycol-Metal Hybrid Nanoparticles and Their Application in Tumor Theranostics. *Adv. Healthc. Mater.* **2022**, *11*, 2200044. [CrossRef]

111. Hou, Y.; Yang, X.; Liu, R.; Zhao, D.; Guo, C.; Zhu, A.; Wen, M.; Liu, Z.; Qu, G.; Meng, H. Pathological Mechanism of Photodynamic Therapy and Photothermal Therapy Based on Nanoparticles. *Int. J. Nanomed.* **2020**, *15*, 6827–6838. [CrossRef] [PubMed]